RSC Advances

PAPER

View Article Online
View Journal | View Issue

Cite this: *RSC Adv.*, 2019, **9**, 40092

Concentration and pump power-mediated color tunability, optical heating and temperature sensing *via* TCLs of red emission in an $Er^{3+}/Yb^{3+}/Li^{+}$ co-doped $ZnGa_2O_4$ phosphor

Monika,[a] Ram Sagar Yadav,*[b] Amresh Bahadur[a] and Shyam Bahadur Rai *[a]

Intense red upconversion luminescence was observed in the $Er^{3+}/Yb^{3+}/Li^{+}$ co-doped $ZnGa_2O_4$ phosphor synthesized through the solid state reaction method for the first time. The structural characterization showed a large crystalline nature and an increase in the particle size *via* Li^{+} doping. The absorption spectra showed a large number of peaks in the UV-vis-NIR regions due to the Er^{3+} and Yb^{3+} ions. The Er^{3+}/Yb^{3+} co-doped $ZnGa_2O_4$ phosphor exhibited green, red and NIR upconversion emissions on excitation with 980 nm radiation. The intensity of the red emission was relatively larger than that of the other emissions. The luminescence intensity *versus* pump power measurements revealed the number of required photons for these emissions. The phosphor showed very interesting color tunability as a function of Er^{3+} ion concentration and incident pump power. The luminescence intensity of the Er^{3+}/Yb^{3+} co-doped phosphor was enhanced more than two times *via* Li^{+} doping. The enhancement in the luminescence intensity was proposed to be due to the increase in the crystallinity and particle size of the phosphor. The lifetimes of the $^4S_{3/2}$ and $^4F_{9/2}$ levels also increased in the presence of Li^{+} ions. The variation in the fluorescence intensity ratio (FIR) of the thermally coupled levels (TCLs) of the red emission with incident pump power offered effective optical heating in the phosphor. The temperature-induced FIR using TCLs of red emission exhibited a larger value of temperature sensing sensitivity in the presence of Li^{+} ions, which was up to 14 $\times$ 10^{-4} K^{-1}. Thus, the $Er^{3+}/Yb^{3+}/Li^{+}$ co-doped $ZnGa_2O_4$ phosphor may be used in photonic, optical heating, and temperature sensing devices.

Received 4th November 2019
Accepted 18th November 2019

DOI: 10.1039/c9ra09120c

rsc.li/rsc-advances

1. Introduction

Optical thermometry is based on the fluorescence intensity ratio (FIR) arising from thermally coupled levels. FIR occurs due to the variation in the upconversion emission intensities between the two thermally coupled levels (TCLs). TCLs are generally found in some of the rare earth ions.[1–4] The rare earth ions exhibit abundant energy levels and result in interesting luminescence of narrow band widths due to the wide range of lifetimes, *i.e.*, from few milliseconds (ms) to microseconds (μs).[5–11] The rare earth-doped upconversion phosphor materials are very encouraging materials and have a large number of technological applications in various fields, such as light-emitting diodes (LEDs), induced optical heating, temperature sensing, chemo-dynamic and photo-dynamic therapy, cancer treatment, bio-thermal treatment, bio-imaging, and theranostics.[12–19] Basically, upconversion is a non-linear optical process, and it is characterized by anti-Stokes emissions, in which two or more low-energy photons are added together and are converted into a high-energy photon.[20–22] Er^{3+} is a rare earth ion, which has been employed as an activator extensively to study upconversion (UC) photoluminescence, UC-based induced optical heating, and temperature sensing sensitivity in different host materials. The Er^{3+} ion has suitable TCLs, which result in a good fit of FIR not only for induced optical heating but also for temperature sensing of phosphor materials.[23–28]

In the UC photoluminescence of Er^{3+}/Yb^{3+} co-doped phosphors, the Er^{3+} ion weakly absorbs an incident near infrared (NIR) 980 nm photon and gives poor UC emission intensity. However, its efficiency can be enriched significantly *via* the doping of Yb^{3+} ions. The Yb^{3+} ion having a large absorption cross-section for NIR light can efficiently absorb it and transfer its excitation energy to the Er^{3+} ion. It has been observed that the UC emission intensity of phosphor materials is also affected by the concentration of the activator ion. The change in the concentration of Er^{3+} ions not only improves the UC emission intensity to a certain extent but also leads to tune colors emitted by the phosphors.[29–33] This type of observation was achieved by

[a]*Laser & Spectroscopy Laboratory, Department of Physics, Institute of Science, Banaras Hindu University, Varanasi 221005, India. E-mail: sbrai49@yahoo.co.in*

[b]*Department of Zoology, Institute of Science, Banaras Hindu University, Varanasi 221005, India. E-mail: ramsagaryadav@gmail.com*

Suo *et al.* in Er^{3+}/Yb^{3+} co-doped $Ba_5Gd_8Zn_4O_{21}$ phosphors.[34] Initially, the Er^{3+} doped $Ba_5Gd_8Zn_4O_{21}$ phosphor emits pure green color. When the Yb^{3+} ion is added in the Er^{3+} doped $Ba_5Gd_8Zn_4O_{21}$ phosphor, the UC emission intensity of the phosphor is enhanced. They also observed color tunability from yellow to reddish yellow regions due to the change in the concentrations of Er^{3+} and Yb^{3+} ions. This occurs due to the shifting of the population of the ions from higher to lower excited states through non-radiative relaxations. Our group has also realized color tunability as a function of Er^{3+} ion concentration in different host matrices.[7,20,28] In these works, green emission is dominant over red emission upon NIR excitation. Inspite of these, the color emitted by a phosphor can also be tuned by increasing the pump power of the 980 nm radiation. Gao *et al.* studied the effect of excitation power and observed color tunability in the $NaYbF_4:X^{3+}$ (X = Er, Ho, and Tm) microcrystal.[35] They also observed a change in the color from green to red, followed by a yellow emission in the $NaYbF_4:Er^{3+}$ microcrystals. Recently, Cheng *et al.* studied the effect of concentration and pump power on the UC emission intensity of Er^{3+}/Yb^{3+} co-doped $ZnGa_2O_4$ and $ZnAl_2O_4$ powder phosphors and obtained only an intense red emission.[36] In the present case, we have studied the UC phenomenon in the Er^{3+}/Yb^{3+} co-doped $ZnGa_2O_4$ phosphor and observed not only an intense red UC emission but also found efficient color tunability due to the change in the concentrations of Er^{3+} ion and pump power of 980 nm radiation.

Nowadays, researchers are encouraged to produce efficient sources of Er^{3+}/Yb^{3+} co-doped phosphor materials by incorporating some additional ions, such as Li^+, Mn^{2+}, Mg^{2+}, Zn^{2+}, Ce^{3+}, and Bi^{3+}.[37–41] They are known as surface modifiers and are helpful in improving the UC emission intensity by modifying the local crystal structure. Out of these ions, the Li^+ ion has been widely incorporated in different combinations of Er^{3+}/Yb^{3+} co-doped phosphor materials.[42–45] It has been noted that the Li^+ ion can easily enter into the sites of host lattices due to its smaller ionic radius and has been proved as a suitable surface modifier. Zhao *et al.* have reported Li^+ ions as a doping element for improving the crystallinity and UC emission intensity in $NaYF_4:Tm^{3+}/Yb^{3+}$ nanoparticles.[46] The addition of Li^+ ions is also found to increase the UC emission intensity of β-$NaYF_4:Er^{3+}/Yb^{3+}$ microparticles.[47] Chen *et al.* have incorporated Li^+ ions in the $Y_2Ti_2O_7:Er^{3+}/Yb^{3+}$ nanophosphor and deduced that the Li^+ ion modifies the local crystal field around the Er^{3+} ion and improves the crystallinity. It also creates oxygen vacancies to maintain charge neutrality in the phosphor.[44] These parameters contributed significantly to the improvement of UC emission intensity of the phosphor. The UC emission intensity of the Er^{3+}/Yb^{3+} co-doped Y_2O_3 nanocrystals is also found to increase due to similar reasons by Li^+ doping.[45] The addition of Cr^{3+} ion in the Er^{3+}/Yb^{3+} co-doped $ZnGa_2O_4$ phosphor led to the improvement of UC emission intensity and the energy transfer from Er^{3+} to Cr^{3+} ions leads to the emission of red color from the Cr^{3+} ion.[48] However, the effect of Li^+ ions on the UC emission intensity of Er^{3+}/Yb^{3+} co-doped $ZnGa_2O_4$ phosphor has still not been studied, to the best of our knowledge.

The thermally coupled levels (TCLs) of rare earth ions are generally separated by a very small energy gap and they lie in the range of 100–2000 cm^{-1}.[3,14] The small energy gap is preferred as it can experience a slight change in the pump power and temperature.[2,14] It has been mentioned earlier that UC emission originating from the TCLs varies non-linearly, as the incident pump power of the exciting source is changed. The non-linear variation in UC emission intensity gives rise to a FIR, which is a direct measure of the optical heating in the phosphor sample.[13,28] The optical heating is generally used in the treatment of infected parts of human organs in which laser guided tools are utilized.[15,19] Optical heating was observed by Du *et al.* in the Er^{3+}/Yb^{3+} co-doped $Na_{0.5}Gd_{0.5}MoO_4$ phosphor, which is a UC-based FIR technique.[13] They have reported that when the pump power of the exciting source is changed, the population of ions is exchanged between the two TCLs. This can generate different values of UC emission intensities from the TCLs. The similar result was also achieved by our group in the Er^{3+}/Yb^{3+} co-doped La_2O_3 phosphor.[28] In this work, we have used TCLs of green emission for obtaining FIR. However, we have used the TCLs of red emission to find FIR in the present work. The optical heating from Er^{3+}/Yb^{3+} ions in the $ZnGa_2O_4$ phosphor is also not investigated in the absence and presence of Li^+ ions, to the best of our knowledge.

On the other hand, optical thermometry has been studied by various researchers in different host materials.[1–4,49–52] The UC-based FIR is a versatile technique in the field of optical thermometry to realize a slight change in the temperature of the desired system without any contact.[14] The UC emission intensity of the TCLs is also affected by changing the external temperature of the phosphor.[1–4] A number of studies was carried out by researchers using Er^{3+}/Yb^{3+} ions in different phosphor materials.[23–28,50] These authors have found FIR by taking UC emission intensities of TCLs of green emission as a function of temperature. It is well known that the $^2H_{11/2}$ and $^4S_{3/2}$ levels of Er^{3+} ion are thermally coupled and they give rise to different values of UC emission intensities as a function of external temperature.[23–28] However, the red emitting ($^4F_{9/2}$) level of Er^{3+} ion also has several Stark components and they are well separated from each other. They can be considered as TCLs and can be used to measure FIR. The Stark components of red emission lie within the range of TCLs (*i.e.*, 165 cm^{-1}).[14] This can yield interesting induced optical heating and temperature sensing observations in the phosphor material. Temperature sensing based on TCLs of green emission has been widely explored.[23–28] However, the impact of red emission is rarely reported for temperature sensing in the Er^{3+}/Yb^{3+} co-doped phosphor.[34] Moreover, Wang *et al.* studied temperature sensing in Ho^{3+}/Yb^{3+} co-doped $Ba_2In_2O_5$ phosphor by treating the Stark components of red emission (*i.e.*, 653 and 661 nm) as TCLs, which are used for calculating the FIR.[3] The temperature sensing characteristics in the Er^{3+}/Yb^{3+} co-doped $ZnGa_2O_4$ phosphor have also not been investigated, to the best of our knowledge, and need a further study.

In order to get more UC emission intensity, a low phonon energy host is preferred. Zinc gallate ($ZnGa_2O_4$) has been used as a host due to its low phonon energy. The low phonon energy

host generally decreases the non-radiative relaxations of the ions occurring in higher lying energy levels. Rare earth doped zinc gallate phosphors have been given much interest due to their wide applications in a variety of fields, such as lighting, field emission display devices (FEDs), and plasma display panels (PDPs).[53–55] It contains an optical band gap of the order of 4.4 eV.[56] $ZnGa_2O_4$ is known as a self-activated host and it emits blue luminescence without doping any activator ion.[57] However, sharp and narrow band emissions are observed in the presence of rare earth ions, such as Er^{3+}, Ho^{3+}, and Eu^{3+} in $ZnGa_2O_4$ phosphors.[58–61] This host is neutral under NIR illumination. When the Er^{3+}/Yb^{3+} ions are co-doped in the $ZnGa_2O_4$ host, it gives intense red UC emission alongwith weak green emission.[36,48] However, the color tunability, induced optical heating, and temperature sensing properties were not explored from Er^{3+}/Yb^{3+} ions in the $ZnGa_2O_4$ phosphor.

In this work, we have selected $ZnGa_2O_4$ as a host due to its low phonon energy. The Er^{3+} and Yb^{3+} ions are co-doped in the $ZnGa_2O_4$ host, which act as acceptor and donor, respectively. The synthesized phosphors are characterized by X-ray diffraction (XRD), scanning electron microscopy (SEM) and energy dispersive X-ray spectroscopic (EDS) techniques to see their structural features. The lattice vibrations in the phosphors have been confirmed by monitoring the Fourier transform infrared (FTIR) spectra. The phosphor sample gives intense red UC emission upon 980 nm excitation. We have observed fine color tunability in the phosphor with different concentrations and incident pump powers. We tried to improve the UC emission intensity of the phosphor by Li^+ doping for the first time. We have calculated FIR of the thermally coupled levels of Er^{3+} ion at different pump powers using two peaks of red emission, *i.e.*, $^4F_{9/2}$(I) and $^4F_{9/2}$(II) at 648 and 655 nm wavelengths, respectively. The FIR (*i.e.*, I_{648nm}/I_{655nm}) was also calculated at different external temperatures in the range of 300–600 K by keeping the pump power of the 980 nm excitation source at 1 W. It has been found that the plots between FIR *versus* pump power and external temperature reveal efficient induced optical heating and temperature sensing properties in the Er^{3+}/Yb^{3+} and $Er^{3+}/Yb^{3+}/Li^{3+}$ co-doped $ZnGa_2O_4$ phosphors. Thus, the possible applications of $Er^{3+}/Yb^{3+}/Li^+$ co-doped $ZnGa_2O_4$ phosphor is suggested in the field of photonic, optical heating, and temperature sensing devices.

2. Experimental

2.1 Synthesis of the phosphor

The $ZnGa_2O_4$:$x$$Er^{3+}/3Yb^{3+}$ phosphors (where x = 0.3, 0.5, 0.7, 1.0, 1.5, and 1.8 mol%) were synthesized by a high temperature solid state reaction method. The host was prepared by using 47 : 53 ratio of ZnO and Ga_2O_3 materials, respectively, as was reported earlier.[57] Stoichiometric amounts of ZnO, Ga_2O_3, Yb_2O_3, and Er_2O_3 materials were weighed precisely. These materials were mixed using an agate mortar and pestle, and acetone was used as the mixing medium. This process was continued for 1 hour to form a homogeneous powder. The mixed powder was placed in a closed furnace maintained at 1200 °C for 5 hours. The similar process was exercised to synthesize (5 mol%) Li^+ doped $ZnGa_2O_4$:$0.7Er^{3+}/3Yb^{3+}$ phosphor using Li_2CO_3 as the doping material. The material thus obtained was crushed and finally produced in the powder form. This is termed as phosphor material and has been used for further measurements at room temperature.

2.2 Characterization

The crystallinity and phase of the synthesized phosphors were confirmed by monitoring the X-ray diffraction (XRD) patterns using Cu Kα radiation (λ = 0.15406 nm) from a MiniFlex 600 (Rigaku, Japan) unit at a scan speed of 2° min^{-1}. The surface morphology of the prepared samples was scanned by scanning electron microscopy (SEM) technique (Zeiss, Evo 18 Research unit). The existence of elements in the phosphor was verified by the energy dispersive X-ray spectroscopic (EDS) analysis. The absorption spectra of the phosphors have been monitored in the range of 200–1100 nm by a PerkinElmer Lambda-750 UV-vis-NIR (ultraviolet-visible-near infrared) spectrometer unit. The Fourier transform infrared (FTIR) spectra of the phosphor samples have been recorded in the range of 400–4000 cm^{-1} using a PerkinElmer IR spectrometer (I-Frontier unit) to see the lattice vibrations of different groups. The UC emission spectra of the phosphor samples have been monitored by using a radiation of 980 nm from a diode laser attached with a PMT (photomultiplier tube) and an iHR320 Horiba Jobin Yvon spectrometer. The lifetime of the $^4S_{3/2}$ and $^4F_{9/2}$ levels of Er^{3+} ion of the phosphors have been monitored by chopping the continuous beam of 980 nm wavelength and a 150 MHz digital oscilloscope (Model no. HM 1507, Hameg instruments). For temperature sensing, the phosphor sample was heated externally by a hot plate stirrer and the temperature of the phosphor sample was measured with the help of a thermo-couple attached with a digital thermometer adjacent to the phosphor sample.

3. Results and discussion

3.1 Structural characterization

3.1.1 XRD measurements. The XRD patterns of $0.7Er^{3+}/3Yb^{3+}$ and $0.7Er^{3+}/3Yb^{3+}/5Li^+$ co-doped $ZnGa_2O_4$ phosphors monitored in the range of 20–80° are shown in Fig. 1. The peaks observed in the XRD patterns match each other, as has been reported earlier.[61] The phase of the phosphor was confirmed to be cubic corresponding to the JCPDS file no. 38-1240. The space group of the phosphor is $Fd\bar{3}m$ (227) with lattice parameters $a = b = c = 8.334$ Å and $\alpha = \beta = \gamma = 90°$. The figure also shows that the phosphors are crystalline in both the cases. When a Li^+ ion is doped at the site of Ga^{3+} ion in $0.7Er^{3+}/3Yb^{3+}$ co-doped $ZnGa_2O_4$ phosphor and the XRD peaks are slightly shifted towards the lower 2θ angle side. It is well known that the ionic radii of the Ga^{3+} ion is 0.62 Å, while that of the Li^+ ion is 0.76 Å. The lattice parameters are expected to increase due to doping of larger ionic radii of Li^+ ions in the $ZnGa_2O_4$ phosphor. It is also clear from the figure that the full width at half maxima (FWHM) of the XRD peak of Li^+ incorporated $0.7Er^{3+}/3Yb^{3+}$ co-doped phosphor is slightly reduced compared to the pure phosphor.

Once the FWHM is reduced *via* incorporation of Li^+ ions in the pure phosphor, it leads to increase crystallinity of the phosphor sample.[44]

The observation of similar shifting was also achieved by our group in the Tb^{3+}/Bi^{3+} co-doped Y_2O_3 phosphor. A shifting in the XRD peaks was observed towards the lower 2θ angle side due larger ionic radii of Bi^{3+} (0.96 Å) compared to Y^{3+} (0.90) ions.[5] It has been also seen that the Bi^{3+} (0.96 Å) ion further leads to a shifting of the XRD peaks towards lower 2θ angle side in the YPO_4 phosphor.[62] In our case, the shifting in the XRD peaks towards lower 2θ angle side and the reduction in FWHM improves the crystallinity of the phosphor significantly.[63] Thus, the Li^+ ion increases the crystallinity of the $0.7Er^{3+}/3Yb^{3+}$ co-doped $ZnGa_2O_4$ phosphor.[44] This could be an encouraging step for obtaining large UC emission intensity in co-doped phosphor materials.

3.1.2 SEM and EDS measurements. The scanning electron microscopic (SEM) images of Er^{3+}/Yb^{3+} and $Er^{3+}/Yb^{3+}/Li^+$ co-doped $ZnGa_2O_4$ phosphors are shown in Fig. 2. The particles of the phosphors are agglomerated in the sample and they are observed with different shapes and sizes. However, the particle shape is found to be nearly rectangular in the case of Er^{3+}/Yb^{3+} co-doped $ZnGa_2O_4$ phosphor (Fig. 2(a)). When the Li^+ ion is doped in the pure phosphor, the particle shape is changed to polyhedral with agglomerated environment and the particle size of the phosphor is also increased. In the presence of Li^+ ions, the porosity of the Er^{3+}/Yb^{3+} co-doped $ZnGa_2O_4$ phosphor is also improved. A similar result was also obtained by our group in which the particle size of the phosphor was increased in the presence of Li^+ ions.[6] It has also been noticed that the addition of Ca^{2+} ion changes the particle shape and size of the Er^{3+} doped phosphor, which are conducive for increasing the corresponding luminescence intensity of the phosphor significantly.[64] In our case, the particle shape and size of the phosphor were changed in the presence of Li^+ ions, which can possibly improve the UC emission intensity of the phosphor sample.

Energy dispersive X-ray spectroscopy (EDS) was used to detect the elements present in the phosphor materials. Fig. 3 shows the EDS spectrum of the $Er^{3+}/Yb^{3+}/Li^+$ co-doped $ZnGa_2O_4$ phosphor. It is clear from the figure that the Zn, Ga, Er, Yb, and O elements are observed in the sample. It also signifies that the elements used during the synthesis are completely incorporated in the phosphor. Li element is not detected in the spectrum because it is a very light element and gets ionized during interaction with the electron beam in the SEM chamber.[65]

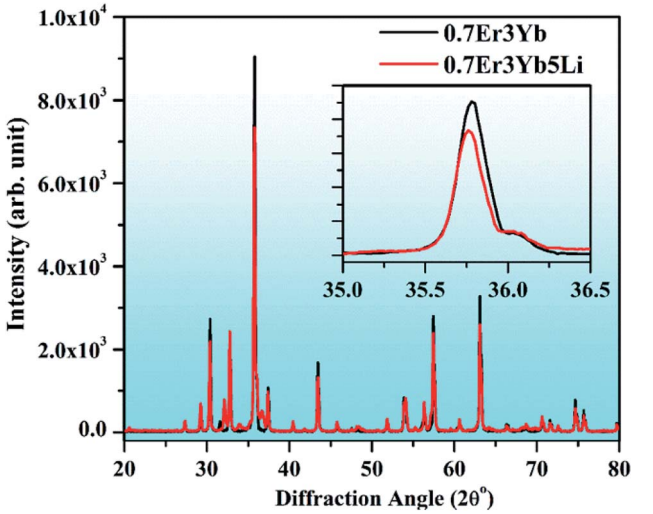

Fig. 1 XRD patterns of $0.7Er^{3+}/3Yb^{3+}$ and $0.7Er^{3+}/3Yb^{3+}/5Li^+$ co-doped $ZnGa_2O_4$ phosphors. The inset figure shows the zoomed XRD patterns in the 35.0–36.5° region.

3.2 FTIR measurements

The FTIR spectra of pure $0.7Er^{3+}$, $xEr^{3+}/3Yb^{3+}$ (*i.e.*, x = 0.3, 0.5, 0.7, 1.0, 1.5, and 1.8 mol%), and $0.7Er^{3+}/3Yb^{3+}/5Li^+$ doped and co-doped $ZnGa_2O_4$ phosphors are shown in Fig. 4. The spectra contain two vibrational bands centered at 440 and 573 cm^{-1}, and these bands are ascribed to the stretching vibrations of Zn–O and Ga–O molecules, respectively.[53] The impurity peaks, such as OH^-, do not appear in the spectra as the phosphor samples were synthesized using high temperature solid state reaction method (at 1200 °C).[7] The intensity of the vibrational bands varies with the increase in the concentration of the dopant ions. Since the phonon energy of the phosphor is small (*i.e.*, 440 and 573 cm^{-1}), it can increase the rate of radiative transitions in the phosphor. Therefore, it may lead to an improvement in the UC emission intensity of the phosphor samples.

3.3 Optical characterization

3.3.1 UV-vis-NIR absorption spectra of the phosphor samples. Fig. 5 shows UV-vis-NIR absorption spectra of the pure $0.7Er^{3+}$, $xEr^{3+}/3Yb^{3+}$ (*i.e.*, x = 0.3, 0.5, 0.7, 1.0, 1.5, and 1.8 mol%), and $0.7Er^{3+}/3Yb^{3+}/5Li^+$ co-doped $ZnGa_2O_4$ phosphors in the range of 200–1100 nm. The spectra show a large number of absorption peaks due to different transitions of Er^{3+} and Yb^{3+} ions. These peaks are centered at 324, 408, 487, 517, 526, 817, and 852 nm, which are attributed to the $^4I_{15/2} \rightarrow {}^4G_{11/2}$, $^2P_{3/2}$, $^4F_{5/2}$, $^2H_{11/2}$, $^4S_{3/2}$, $^4F_{9/2}$, and $^4I_{9/2}$ transitions of Er^{3+} ions, respectively.[23–28] The spectra also contain an intense band at 972 nm in the NIR region and it is due to the $^2F_{7/2} \rightarrow {}^2F_{5/2}$ transition of the Yb^{3+} ion.[2,7,28]

When the Li^+ ion is incorporated in the Er^{3+}/Yb^{3+} co-doped phosphor, the intensity of the absorption bands is slightly improved. It is also noticed from the figure that there is an additional band observed in the 200–350 nm region. This is due to the charge transfer state (CTS) transitions of O^{2-}–Ga^{3+} and O^{2-}–Zn^{2+} ions at 254 and 325 nm wavelengths, respectively.[53] This figure also shows that the intensity of the NIR band is also increased in the presence of Li^+ ions. This verifies that the Yb^{3+} ion has better absorption cross section in this region. In fact, the Yb^{3+} ion absorbs NIR wavelength (*i.e.*, 980 nm) efficiently and transfers its energy to the Er^{3+} ion, which can yield larger UC emission intensity.[2,6,7]

3.3.2 Optical band gap analysis. The UV-vis-NIR absorption data have been monitored in the K–M (Kubelka–Munk) mode and used to calculate the optical band gap of the phosphors.

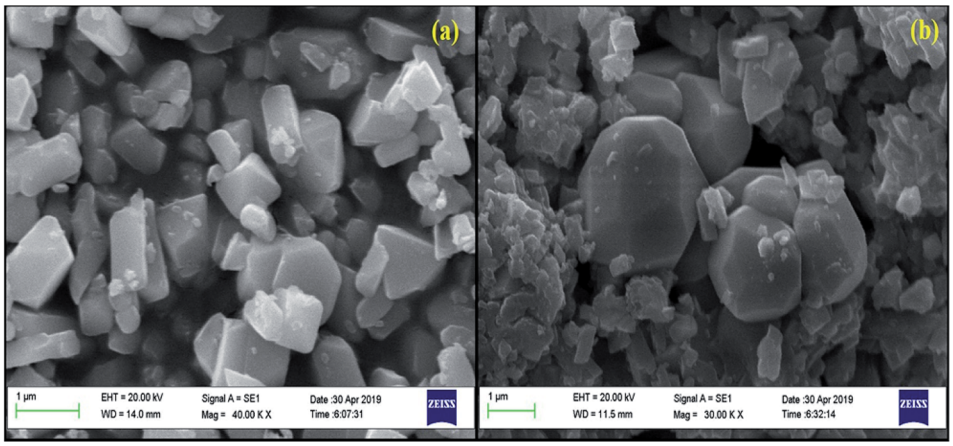

Fig. 2 SEM images of the (a) Er^{3+}/Yb^{3+} and (b) $Er^{3+}/Yb^{3+}/Li^{+}$ co-doped $ZnGa_2O_4$ phosphors.

The optical band gap of the phosphor samples was calculated by using Wood and Tauc formula:[5,66]

$$\alpha = \frac{B(h\nu - E_g)^n}{h\nu} \quad \text{(i)}$$

where α is the absorption coefficient, B is the band tailoring constant, h is a Planck's constant, ν is the frequency of the incident photon, and E_g is the optical band gap energy. The value of n is taken as 1/2 for direct band gap calculation. We have observed the plots between $(\alpha h\nu)^2$ *versus* $h\nu$ for the $0.7Er^{3+}$, $0.7Er^{3+}/3Yb^{3+}$, and $0.7Er^{3+}/3Yb^{3+}/5Li^{+}$ doped and co-doped $ZnGa_2O_4$ phosphors and the optical band gap thus obtained is shown in Fig. 6. The optical band gap is found to be 4.87 eV for the $0.7Er^{3+}$ doped phosphor (see Fig. 6(a)). This value of optical band gap matches with the earlier reported value for the $ZnGa_2O_4$ phosphor.[56] When the Yb^{3+} ion is also co-doped in the $0.7Er^{3+}$:$ZnGa_2O_4$ phosphor, the optical band gap is slightly reduced to 4.75 eV (see Fig. 6(b)).

The presence of Li^{+} ions alongwith Er^{3+} and Yb^{3+} in the phosphor further reduces the value of the optical band gap to 4.68 eV (see Fig. 6(c)). It has been also observed by our group that the optical band gap of the La_2O_3 phosphor is reduced significantly in the presence of Bi^{3+} ion.[7] Once the optical band gap is reduced, a large number of excited ions may be promoted to higher lying energy levels. As discussed earlier, Li^{+} doping also improved the crystallinity and the particle size of the phosphor. Therefore, the UC emission intensity of the phosphor is expected to be enhanced in the presence of Li^{+} ions due to these reasons.

3.3.3 UC photoluminescence under 980 nm excitation. The UC emission spectra of the $0.7Er^{3+}$ and $0.7Er^{3+}/3Yb^{3+}$ doped and co-doped $ZnGa_2O_4$ phosphors monitored in the range of 350–850 nm on excitation with 980 nm at 1 W are shown in Fig. 7. The spectra contain a large number of UC peaks centered at 380, 407, 487, 524, 554, (655 and 674), and (789 and 814) nm, and these peaks are attributed to the ($^4G_{11/2} \rightarrow {}^4I_{15/2}$), ($^2P_{3/2} \rightarrow {}^4I_{13/}$

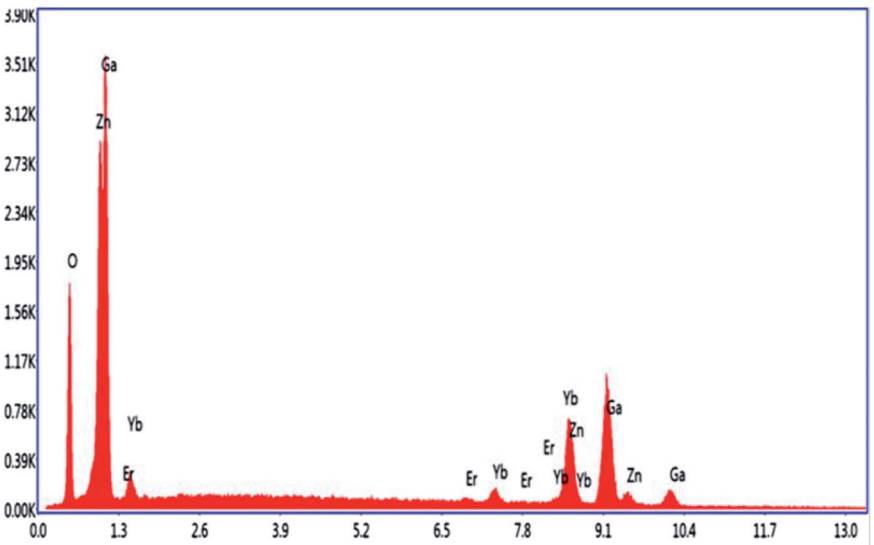

Fig. 3 EDS spectrum of the $Er^{3+}/Yb^{3+}/Li^{+}$ co-doped $ZnGa_2O_4$ phosphor.

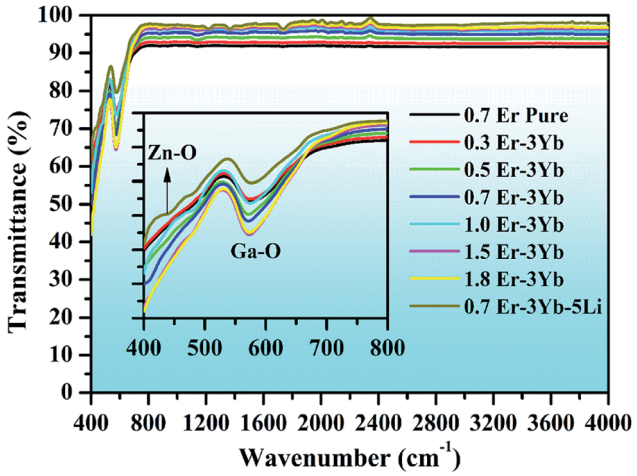

Fig. 4 FTIR spectra of $0.7Er^{3+}$, $xEr^{3+}/3Yb^{3+}$ (*i.e.*, $x = 0.3$, 0.5, 0.7, 1.0, 1.5, and 1.8 mol%), and $0.7Er^{3+}/3Yb^{3+}/5Li^{+}$ co-doped $ZnGa_2O_4$ phosphors.

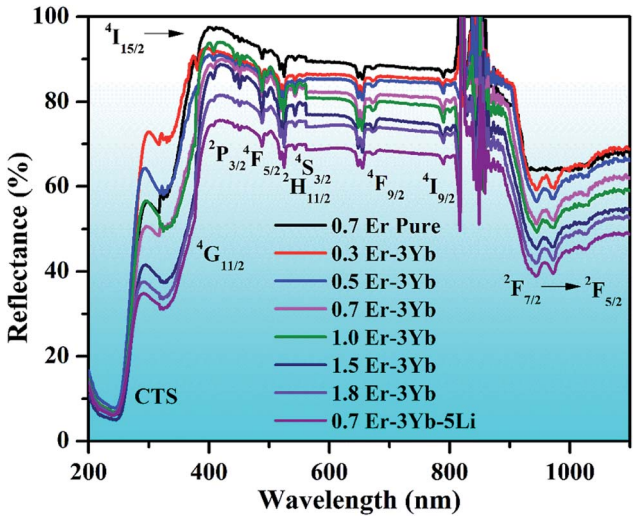

Fig. 5 UV-vis-NIR spectra of $0.7Er^{3+}$, $xEr^{3+}/3Yb^{3+}$ (*i.e.*, $x = 0.3$, 0.5, 0.7, 1.0, 1.5, and 1.8 mol%), and $0.7Er^{3+}/3Yb^{3+}/5Li^{+}$ co-doped $ZnGa_2O_4$ phosphors.

$_2$), ($^4F_{5/2} \rightarrow {}^4I_{15/2}$), ($^2H_{11/2} \rightarrow {}^4I_{15/2}$), ($^4S_{3/2} \rightarrow {}^4I_{15/2}$), ($^4F_{9/2} \rightarrow {}^4I_{15/2}$), and ($^4I_{9/2} \rightarrow {}^4I_{15/2}$) transitions of the Er^{3+} ion, respectively.[7,23–28] The peaks observed in the two cases match to each other. All the emission peaks are also split into well separated Stark components.[28] This is due to the presence of a strong crystal structure around the Er^{3+} ion. Fig. 7(b) and (c) are the zoomed part of the spectra of the phosphors in the near UV-blue and NIR regions, respectively. They also show significant splitting in these emission peaks.

The phosphor gives intense red emission alongwith weak near UV, blue, green, and NIR emissions. However, some of the emission peaks are not clearly seen in the $0.7Er^{3+}$ doped phosphor. These peaks can be achieved *via* doping of the Yb^{3+} ion. When the Yb^{3+} ion is doped in the $0.7Er^{3+}$:$ZnGa_2O_4$ phosphor, the emission peaks in the near UV and blue regions are observed with significant UC emission intensity. This is due to efficient energy transfer from Yb^{3+} to Er^{3+} ions.[28] The UC intensity of the $0.7Er^{3+}$ doped phosphor is enhanced up to 42 times for the red emission (at 655 nm) in the presence of Yb^{3+} ion. However, the enhancement factor is relatively small for the other emission peaks, *i.e.*, 25, 23, 5, and 3 times for 407, 524, 554, and 814 nm, respectively. The occurrence of intense red UC emission is due to energy back transfer and cross relaxation among the Er^{3+} ions.[30] Zhang *et al.* have also reported strong red emission due to cross relaxation in the Er^{3+}/Yb^{3+} co-doped Y_2O_3 phosphor.[32]

In order to optimize the UC emission intensity of the $xEr^{3+}/3Yb^{3+}$ co-doped $ZnGa_2O_4$ phosphors, the phosphor samples have been synthesized with different concentrations of Er^{3+} ions (*i.e.*, $x = 0.3$, 0.5, 0.7, 1.0, 1.5, and 1.8 mol%). When the $xEr^{3+}/3Yb^{3+}$ co-doped phosphor samples are excited by 980 nm at 1 W, the UC emission intensity of the phosphor initially increases with increase in the concentration of Er^{3+} ions. It is found to increase up to 0.7 mol% concentration of Er^{3+} ions. When the concentration of Er^{3+} ions is further increased, the UC emission intensity decreases due to concentration quenching effect. Li *et al.* also observed optimum emission intensity at 0.7 mol% concentration of Er^{3+} ions in the Yb^{3+}/Er^{3+} co-doped $BaZrO_3$ ceramics and after this, they reported a decrease in the UC intensity.[67] Our group has also found the optimum concentration of the Er^{3+} ion at 0.7 mol% in the $Tm^{3+}/Er^{3+}/Yb^{3+}$ co-doped Y_2O_3–ZnO nano-composite.[20]

Generally, the concentration quenching occurs at higher concentrations of the dopant ions. In concentration quenching, the inter-ionic separation between the Er^{3+} ions seems to be closer than the critical separation and the excitation energy migrates to the energy killing sites; thereby, a decrease in the UC intensity is observed.[20,67] The effect of concentration of Er^{3+} ion on the UC intensity of the $xEr^{3+}/3Yb^{3+}$ co-doped $ZnGa_2O_4$ phosphors ($x = 0.3$, 0.5, 0.7, 1.0, 1.5, and 1.8 mol%) is shown in Fig. 8(a–c). It is also clear from the figure that the UC emission intensity of the co-doped phosphor is optimum at 0.7 mol% concentration of the Er^{3+} ions. The color emitted by the phosphor leads to tune from greenish yellow to yellowish green color with the increase in the concentration of Er^{3+} ions, which is to be discussed in the following section. These emissions originate due to different excitation processes, such as ground state absorption (GSA), excited state absorption (ESA), energy transfer upconversion (ETU), cooperative energy transfer (CET), cross relaxation (CR), and back energy transfer (EBT). The inset in Fig. 8(a) shows the red to green (R/G) ratio for different concentrations of Er^{3+} ions. This ratio decreases regularly with increasing concentration and finally saturates at higher concentrations of Er^{3+} ions. A comparison of color tunability for different concentrations of Er^{3+} ions have been summarized in Table 1 in terms of CIE coordinates.

Fig. 9 shows the schematic energy level diagram of Er^{3+} and Yb^{3+} ions and the mechanisms involved in the UC emission processes, *i.e.*, GSA, ESA, ETU, CET, CR, and EBT. When the single Er^{3+} doped $ZnGa_2O_4$ phosphor is excited by 980 nm radiation, the Er^{3+} ions absorb this radiation weakly in the ground level ($^4I_{15/2}$). Due to this, these ions are promoted to the

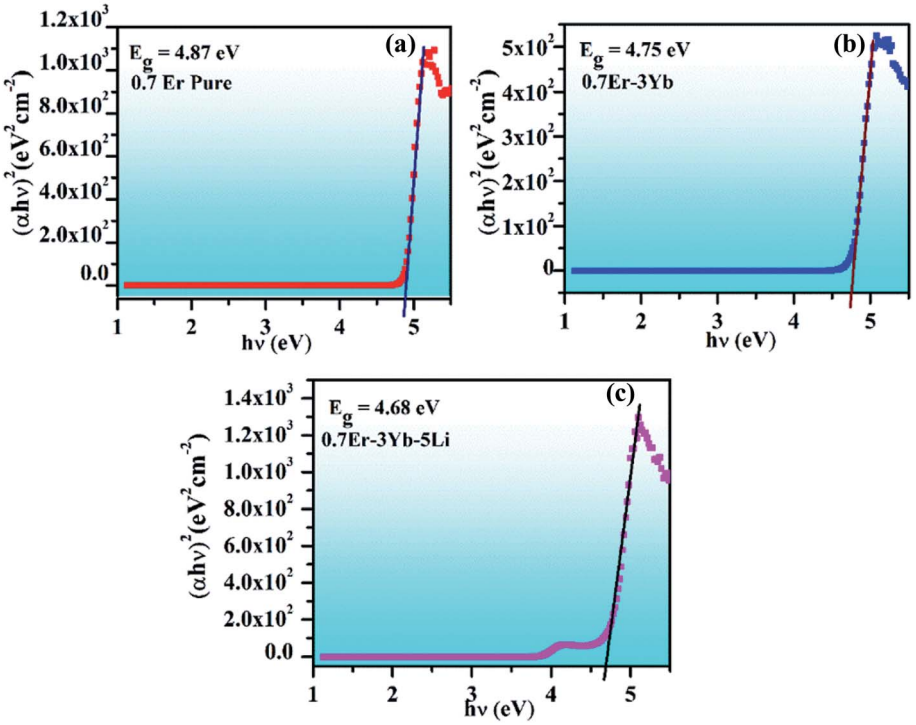

Fig. 6 Plots between $(\alpha h\nu)^2$ *versus* $h\nu$ for the (a) $0.7Er^{3+}$, (b) $0.7Er^{3+}/3Yb^{3+}$, and (c) $0.7Er^{3+}/3Yb^{3+}/5Li^{+}$ doped and co-doped $ZnGa_2O_4$ phosphors.

$^4I_{11/2}$ level of the Er^{3+} ion and this process is called ground state absorption (GSA). The ions in the $^4I_{11/2}$ level further absorb another 980 nm photon and are promoted to the $^4F_{7/2}$ level through excited state absorption (ESA). These ions are further promoted from $^4F_{7/2}$ to $^2P_{3/2}$ level *via* the absorption of another (third) 980 nm photon. On relaxation, these ions populate the

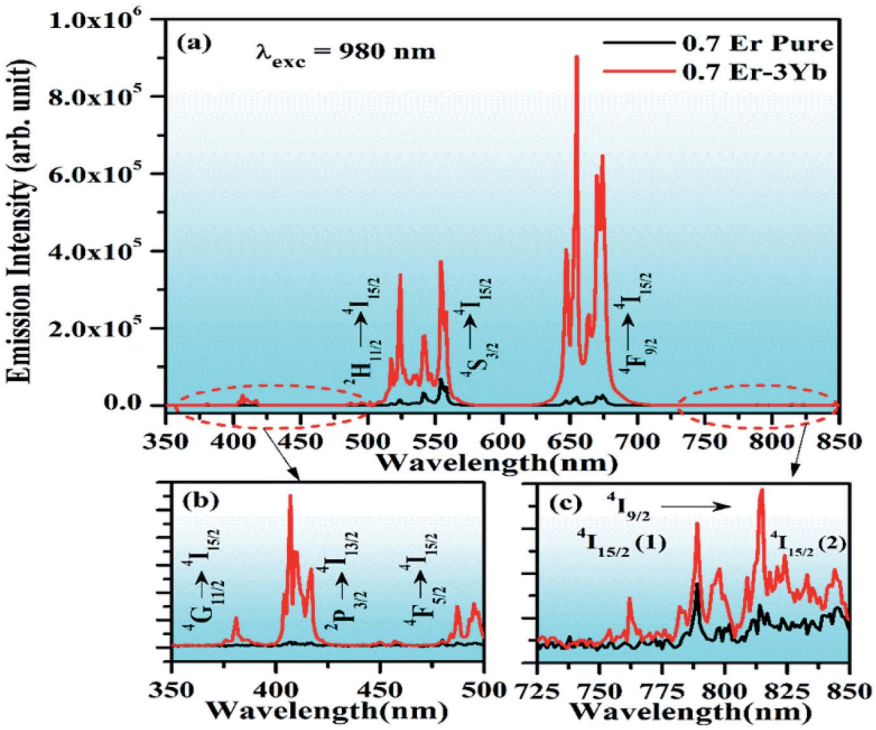

Fig. 7 (a) UC emission spectra of the $0.7Er^{3+}$ and $0.7Er^{3+}/3Yb^{3+}$ doped and co-doped $ZnGa_2O_4$ phosphors on excitation with 980 nm at 1 W. The figures (b) and (c) are the zoomed spectra in the near UV-blue and NIR regions, respectively.

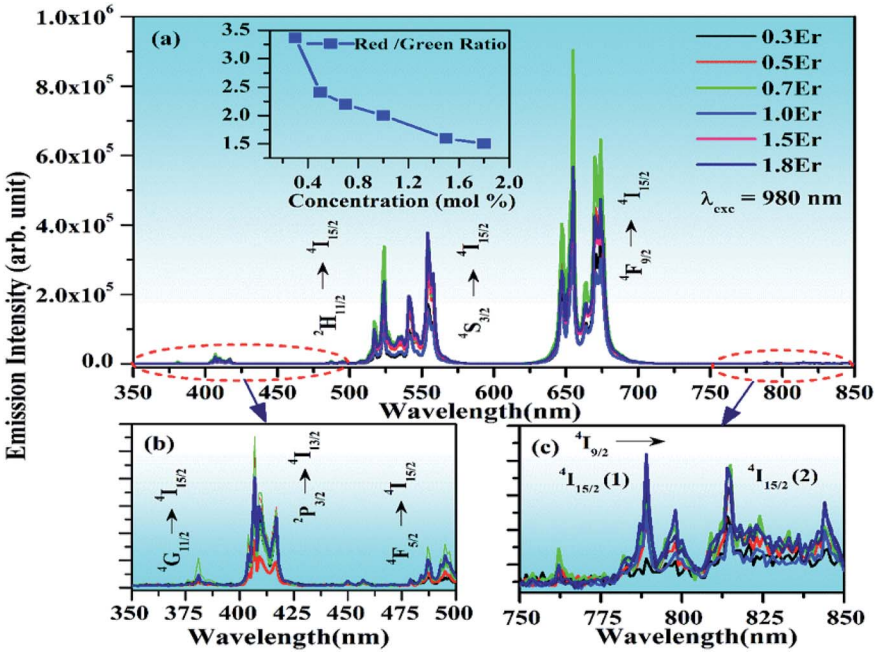

Fig. 8 (a) Effect of concentration of Er^{3+} ion on the UC intensity of $xEr^{3+}/3Yb^{3+}$ co-doped $ZnGa_2O_4$ phosphors (where $x = 0.3$, 0.5, 0.7, 1.0, 1.5, and 1.8 mol%) on excitation with 980 nm at 1 W. The figures (b) and (c) are the zoomed spectra in the near UV-blue and NIR regions, respectively. The inset in (a) is a variation of red to green ratio (R/G) for different concentrations of Er^{3+} ions.

$^2H_{11/2}$, $^4S_{3/2}$, $^4F_{9/2}$, and $^4I_{9/2}$ levels strongly due to non-radiative relaxations.[23–28] As a result, they give radiative transitions at 380, 524, 554, (655, 674), and 814 nm wavelengths to different low-lying levels including the ground state (see Fig. 9). The emissions in the near UV and blue regions are not observed clearly as the upper energy levels corresponding to these emissions are weakly populated in the pure phosphor.

When the Yb^{3+} ion is doped in the Er^{3+}:$ZnGa_2O_4$ phosphor, it transfers its excitation energy to Er^{3+} ions through ETU (energy transfer upconversion) and CET (cooperative energy transfer) processes (see Fig. 9). It leads to the populations of ions in some of those energy levels in which the population was not achieved considerably, as was discussed in the pure case. Actually, when the Er^{3+}/Yb^{3+} co-doped $ZnGa_2O_4$ phosphor is excited with 980 nm radiation, the Yb^{3+} ions are promoted from the ground ($^2F_{7/2}$) level to the excited ($^2F_{5/2}$) level through GSA. The ions in the $^2F_{5/2}$ level relax to the ground level non-radiatively and transfer their excitation energy to different energy levels of the Er^{3+} ion, *i.e.*, $^4I_{11/2}$, $^4F_{7/2}$, and $^2P_{3/2}$ levels due to energy transfer upconversion (ETU) process. There is also an energy transfer from Yb^{3+} to Er^{3+} ions in the $^4F_{7/2}$ level through cooperative energy transfer (CET) process. The ions in this level are further promoted to the $^2P_{3/2}$ level through ESA. Finally, the $^4G_{11/2}$ and $^4F_{5/2}$ levels are populated *via* non-radiative relaxations alongwith other low-lying levels.[7] The ions in $^2P_{3/2}$, $^4G_{11/2}$, and $^4F_{5/2}$ levels produce radiative transitions at different wavelengths, such as 381, 407, and 487 nm, respectively. These transitions appear very weakly in the Er^{3+} doped phosphor (see Fig. 7). The Er^{3+}/Yb^{3+} co-doped phosphor also gives radiative emissions at 524, 554, (655, 674), and 814 nm wavelengths upon 980 nm excitation.[28]

On the other hand, the intense red UC emission occurs due to energy back transfer (EBT) and cross relaxation (CR) between Er^{3+} and Yb^{3+} ions.[30,32,34] In the EBT process, the energy transfer

Table 1 Variation in CIE coordinates with different concentrations of Er^{3+} ions and at different pump powers of the 980 nm excitation source

Concentration (mol%)	CIE coordinates (x, y)	Pump power (W) for $0.7Er^{3+}/3Yb^{3+}$ phosphor	CIE coordinates (x, y)
0.7Er	0.33, 0.62	0.30 W	0.42, 0.41
0.3Er–Yb	0.41, 0.55	0.50 W	0.45, 0.51
0.5Er–Yb	0.39, 0.58	0.70 W	0.44, 0.53
0.7Er–Yb	0.38, 0.59	0.90 W	0.43, 0.54
1.0Er–Yb	0.39, 0.57	1.10 W	0.42, 0.55
1.5Er–Yb	0.37, 0.60	1.30 W	0.42, 0.56
1.8Er–Yb	0.37, 0.60	1.50 W	0.41, 0.57
0.7Er–Yb–Li	0.39, 0.58	1.70 W	0.40, 0.57

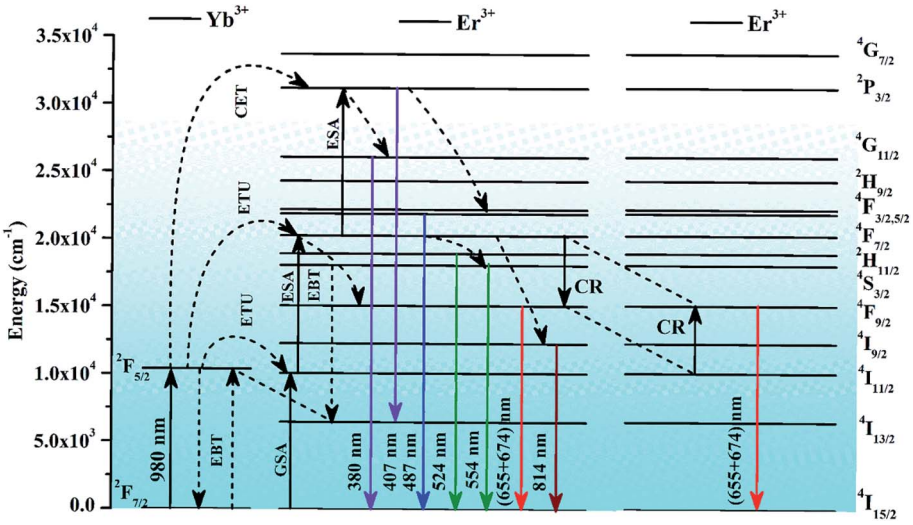

Fig. 9 Schematic energy level diagram of Er^{3+} and Yb^{3+} ions, and the mechanisms involved in different transitions.

takes place from $^4S_{3/2}$ to $^4I_{13/2}$ levels of the Er^{3+} ions and $^2F_{7/2}$ to $^2F_{5/2}$ levels of the Yb^{3+} ions as Er^{3+} ($^4S_{3/2}$) + Yb^{3+} ($^2F_{7/2}$) → Er^{3+} ($^4I_{13/2}$) + Yb^{3+} ($^2F_{5/2}$). It populates the $^2F_{5/2}$ level of the Yb^{3+} ion followed by depopulation of the $^4S_{3/2}$ level of Er^{3+} ion. Once the population in the $^4S_{3/2}$ level is reduced, the intensity of green emission at 554 nm decreases considerably. There is another reason for the decrease in the green emission intensity, which is due to cross relaxation (CR) process.[30,68] It is well known that the energy separation between $^4F_{7/2}$ and $^4F_{9/2}$ levels of Er^{3+} ion is 5200 cm^{-1} while that between $^4I_{11/2}$ and $^4F_{9/2}$ levels is 5100 cm^{-1}. This energy separation can easily generate CR between these levels. This promotes the large population of Er^{3+} ions in the $^4F_{9/2}$ level as Er^{3+} ($^4F_{7/2}$) + Er^{3+} ($^4I_{11/2}$) → Er^{3+} ($^4F_{9/2}$) + Er^{3+} ($^4F_{9/2}$). As a result, a relatively larger intensity of red

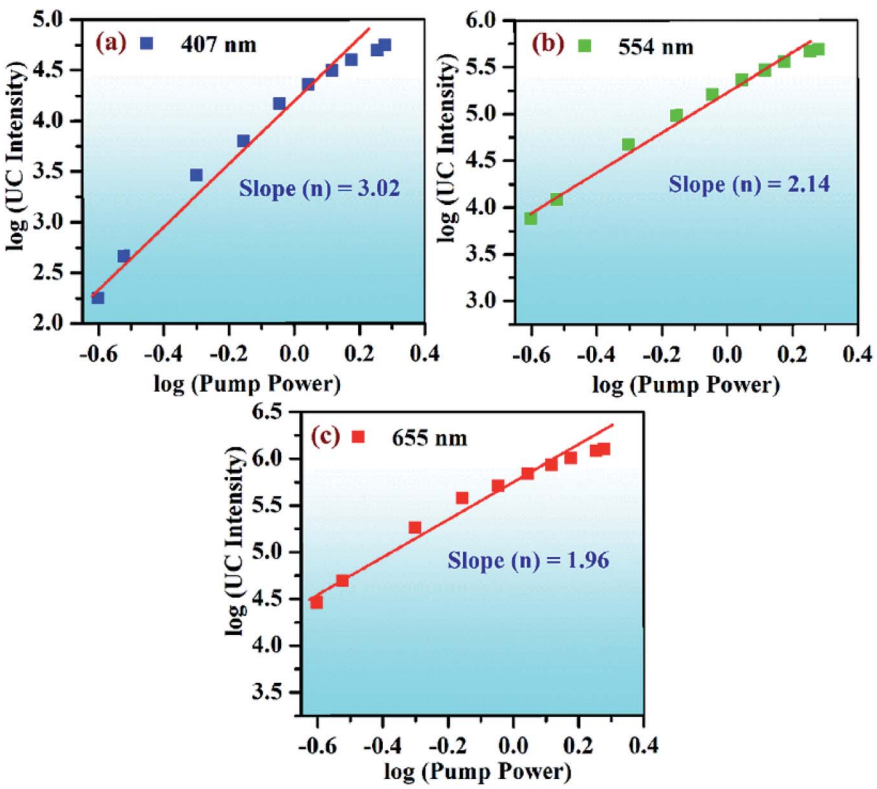

Fig. 10 Dual logarithm plots between pump power *versus* UC emission intensity for (a) blue, (b) green, and (c) red emissions of the Er^{3+}/Yb^{3+} co-doped $ZnGa_2O_4$ phosphor annealed (at 1200 °C 5 h^{-1}) under 980 nm excitation.

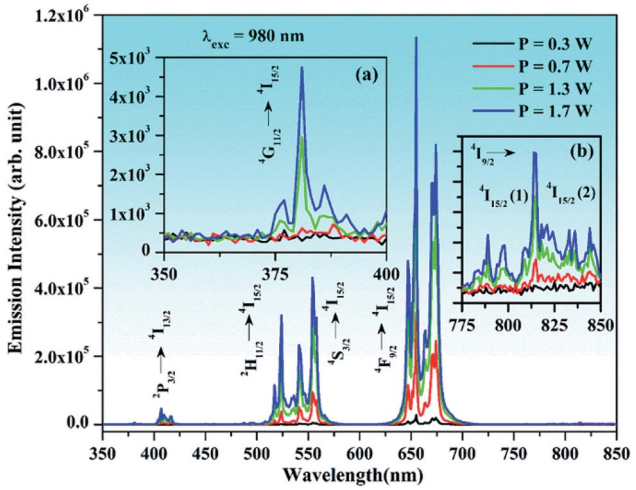

Fig. 11 Effect of incident pump power on the UC emission intensity of $0.7Er^{3+}/3Yb^{3+}$ co-doped $ZnGa_2O_4$ phosphor at 0.3, 0.7, 1.3, and 1.7 W. The inset (a) is the zoomed spectra in the near UV region whereas the inset (b) shows spectra in the NIR region, respectively.

emission is observed compared to the green emission and it varies with the increase in the concentration of Er^{3+} ions.

3.3.4 Effect of pump power on UC emission intensity of $0.7Er^{3+}/3Yb^{3+}$ co-doped phosphor. In the upconversion process, the UC emission intensity (I_{up}) is directly proportional to n^{th} power of the incident pump power as $I_{up} \propto P^n$, where n is the number of absorbed photons. Fig. 10 shows dual logarithmic plots between UC emission intensity (I_{up}) and incident pump power for 407, 554, and 655 nm wavelengths, which yield a straight line and they have been used to calculate the slope values (n). The slope values thus calculated were found to be 3.02, 2.14, and 1.96 for the blue (407 nm), green (554 nm), and red (655 nm) emissions, respectively. These values suggest that the blue emission is observed due to absorption of three photons whereas the green and red emissions are due to absorption of two photons.[20] The three photons are also involved in the population of the $^2P_{3/2}$ level, which is responsible for 407 nm emission whereas two photons are used to populate the $^4S_{3/2}$ and $^4F_{9/2}$ levels of Er^{3+} ions, emitting 554 and 655 nm emissions, respectively. The deviations from an integral value are due to involvement of non-radiative channels in different energy levels.

The UC emission intensity of the Er^{3+}/Yb^{3+} co-doped phosphor was monitored at different pump powers, *i.e.*, 0.3, 0.7, 1.3, and 1.7 W, and they are shown in Fig. 11. This facilitates to see the effect of incident pump powers on the UC emission intensity of the co-doped phosphor. It is clear from the figure that the UC emission intensity of $0.7Er^{3+}/3Yb^{3+}$ co-doped phosphor increases continuously on increasing the pump power of NIR radiation (*i.e.*, 980 nm). Initially, at 0.3 W pump power, the emissions in the near UV-blue and NIR regions are not observed. However, these emissions can be seen clearly when

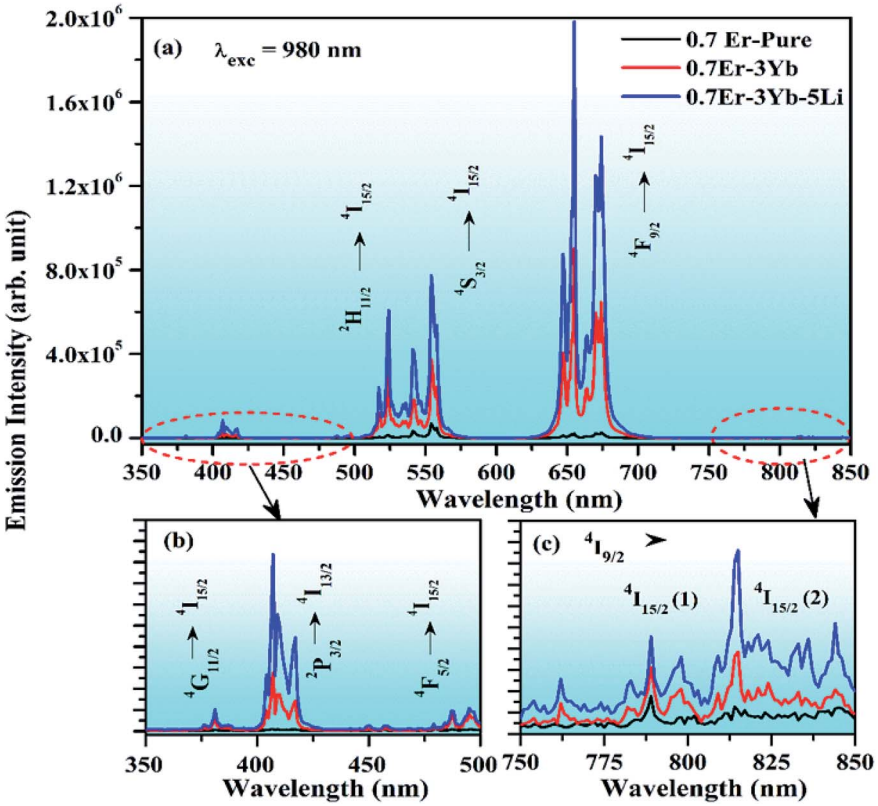

Fig. 12 (a) Comparison in UC emission intensity of $0.7Er^{3+}$ (pure), $0.7Er^{3+}/3Yb^{3+}$, and $0.7Er^{3+}/3Yb^{3+}/Li^+$ doped and co-doped $ZnGa_2O_4$ phosphors on excitation with 980 nm. Figures (b) and (c) are the UC emission spectra in the near UV-blue and NIR regions, respectively.

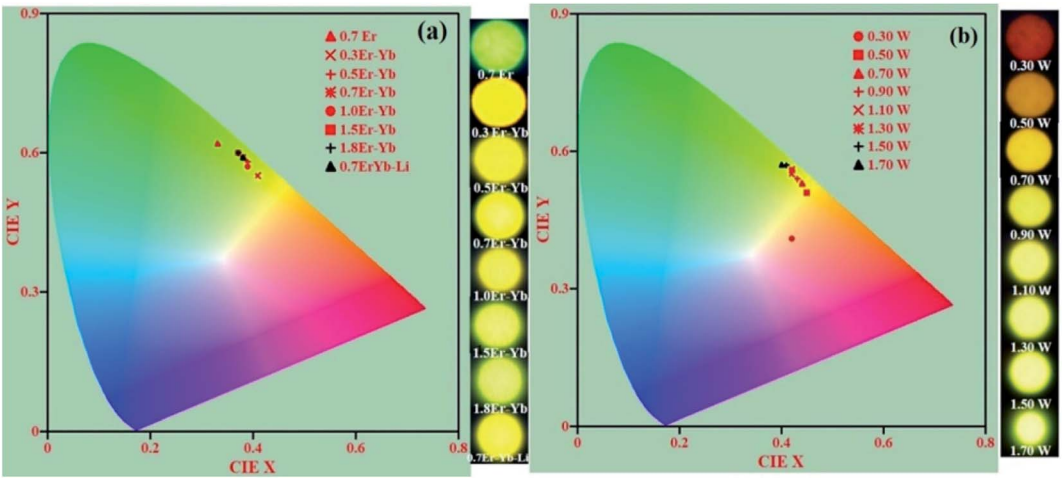

Fig. 13 CIE diagrams of the $Er^{3+}/Yb^{3+}/Li^{+}$ co-doped $ZnGa_2O_4$ phosphors with the variation in (a) concentrations of the Er^{3+} ions and (b) incident pump powers of the 980 nm radiation.

the pump power is increased to 0.7 W. The emission intensity is further increased at higher pump powers, *i.e.*, 1.3 and 1.7 W.[25,67] This is due to the fact that at lower pump power, the upper lying excited levels are not populated, while the population of the ions is effectively established in these levels at higher pump power.

Fig. 11(a) shows that emission in the near UV region begins to appear at higher pump powers (*i.e.*, 1.7 W) as the upper lying energy levels are populated. However, in the NIR region, it arises even at relatively lower pump power (see Fig. 11(b)). The low-lying energy levels are generally populated even at lower pump power and give NIR emissions.

3.3.5 Effect of Li^{+} ions on UC emission intensity of $0.7Er^{3+}/3Yb^{3+}$ co-doped phosphor. The phosphor sample was synthesized with 5 mol% concentrations of Li^{+} ions in order to enhance the UC emission intensity of the phosphor. The concentration of the dopant ion strongly affects the UC emission intensity of the phosphor. The effect of Li^{+} ions on the UC emission intensity of the $0.7Er^{3+}/3Yb^{3+}$ co-doped $ZnGa_2O_4$ phosphor monitored in the range of 350–850 nm upon 980 nm excitation is shown in Fig. 12. The spectra contain similar emission peaks with very large emission intensity. The UC emission intensity of the red emission band is enhanced up to 90 times in the presence of Li^{+} ions compared to the $0.7Er^{3+}$ doped phosphor. However, the UC emission intensity of the $0.7Er^{3+}/3Yb^{3+}$ co-doped phosphor is enhanced more than two times in the presence of Li^{+} ions. This enhancement in the UC emission intensity is due to several factors, such as improvement in crystallinity, particles size, increase in absorption cross section, and reduction in optical band gap.

As was mentioned earlier, the addition of some surface modifiers greatly affects the intensity of different phosphor materials, *e.g.*, Li^{+}, Mn^{2+}, Mg^{2+}, Zn^{2+}, Ce^{3+}, and Bi^{3+}.[37–41] It has been observed earlier that they enhance the intensity of the materials by modifying the local crystal field around the activator ions.[6,69] The modification in the local crystal field is achieved when larger ionic radii ion is incorporated at the sites of smaller ionic radii ion. It is expected that the incorporation of

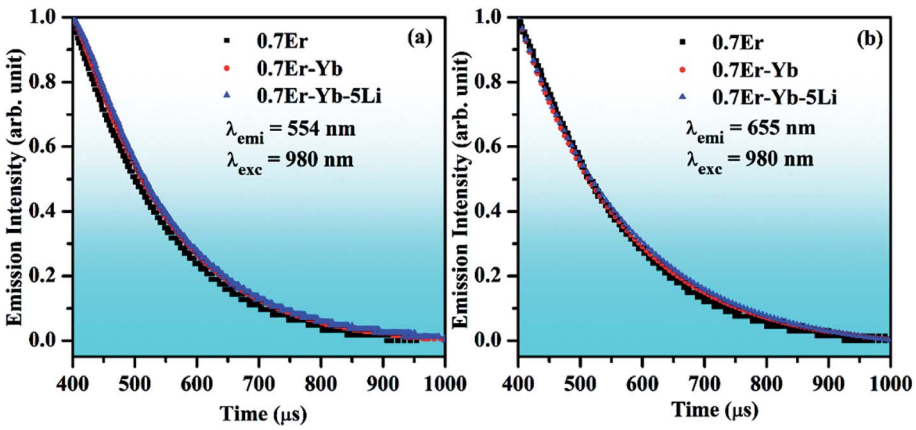

Fig. 14 Decay curves of (a) $^4S_{3/2}$ level (554 nm) and (b) $^4F_{9/2}$ level (655 nm) of Er^{3+} ion for the $0.7Er^{3+}$, $0.7Er^{3+}/Yb^{3+}$, and $0.7Er^{3+}/Yb^{3+}/Li^{+}$ doped and co-doped $ZnGa_2O_4$ phosphors on excitation with 980 nm.

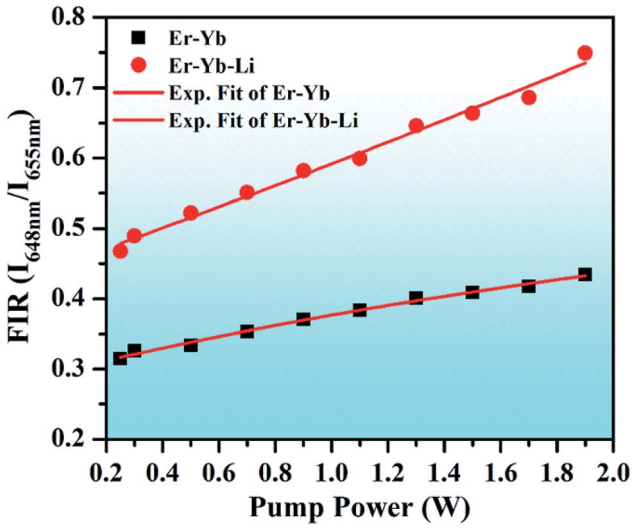

Fig. 15 Variation of FIR (I_{648nm}/I_{655nm}) *versus* incident pump powers for the 0.7Er^{3+}/Yb^{3+} and 0.7Er^{3+}/Yb^{3+}/Li^{+} co-doped $ZnGa_2O_4$ phosphors upon 980 nm excitation.

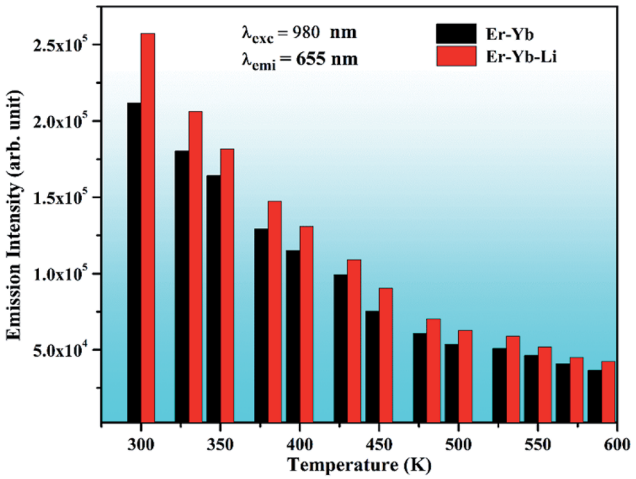

Fig. 16 Variation in the UC emission intensity *versus* external temperature for 655 nm emission band in the 0.7Er^{3+}/Yb^{3+} and 0.7Er^{3+}/Yb^{3+}/Li^{+} co-doped $ZnGa_2O_4$ phosphors upon 980 nm excitation at 1 W pump power.

the larger sized ion creates an expansion in the crystal lattice parameters and thereby improves the intensity of the phosphor materials.[5] A similar result has been obtained in our case in which the Li^{+} ion with larger ionic radii is substituted at the site of the Ga^{3+} ion in the host lattice. This reduces the FWHM of the XRD peaks, which confirms an increase in the crystallinity of the phosphor samples. The SEM micrographs also reveal an increase in the particle size in the presence of Li^{+} ions. These factors contributed significantly in enhancing the UC emission intensity.

The incorporation of Li^{+} ions increases the absorption of vibrational bands of the host lattice. This indicates that the local crystal field has less surface defects.[31] This was also confirmed from the XRD analysis, as the crystal structure becomes more crystalline in the presence of Li^{+} ions. It was also analyzed from the UV-vis-NIR spectra that the emission intensity of the NIR band is enhanced significantly in the presence of Li^{+} ions. It is also interesting to notice that the optical band gap of the phosphor is slightly reduced *via* Li^{+} doping. On the other hand, the lifetime of the emitting levels is increased considerably in the presence of Li^{+} ions.[6] Chen *et al.* have studied the effect of Li^{+} ions in the red UC emission intensity of Er^{3+} ion and found manifold enhancement due to an increase in the crystallinity of the phosphor.[44] The effect of the addition of Li^{+} ions was also studied by Huerta *et al.*; they found an increase in the red UC emission intensity, which occurs due to increase in the crystallinity of the phosphor.[70] Liu *et al.* have also observed an intense red color due to energy back transfer and cross relaxation processes. They have obtained larger intensity in the presence of F^{-} ion.[71] The enhancement was also observed due to an increase in the crystallinity of the phosphor *via* F^{-} doping. In our case, the increase in crystallinity and particle size, enhancement in absorption and reduction in optical band gap collectively improve the population of the excited ions in different higher energy levels, which results in an enhancement in the red UC emission intensity of the phosphor more than two times. Fig. 12(b) and (c) shows that the UC emission intensity of the phosphor was improved significantly in the near UV-blue and NIR regions in the presence of Li^{+} ions.

The CIE (Commission International de l'Eclairage) coordinates are a suitable way to specify the emitted color, which involve x and y parameters specifying the hue and saturation natures in two dimensions. The obtained CIE coordinates are indicated in the chromaticity diagram. Fig. 13(a) and (b) show the CIE diagrams of $x$$Er^{3+}$/3$Yb^{3+}$/5$Li^{+}$ with different concentrations (*i.e.*, x = 0.3, 0.5, 0.7, 1.0, 1.5, & 1.8 mol%) and that of 0.7Er^{3+}/3Yb^{3+} co-doped $ZnGa_2O_4$ phosphors at different pump powers (*i.e.*, 0.3, 0.5, 0.7, 0.9, 1.10, 1.30, 1.50, and 1.70 W) of the 980 nm excitation source. The color co-ordinates lie in the green region for the 0.7Er^{3+} doped phosphor; however, the emitted color of the 0.3Er^{3+}/3Yb^{3+}, 0.5Er^{3+}/3Yb^{3+}, 0.7Er^{3+}/3Yb^{3+}, 1.0Er^{3+}/3Yb^{3+}, 1.5Er^{3+}/3Yb^{3+}, and 1.8Er^{3+}/3Yb^{3+} co-doped phosphors changes from yellow to greenish yellow regions. It suggests that the color of the phosphor is tunable on increasing the concentration of the Er^{3+} ion.[34] The CIE coordinates thus calculated are summarized in Table 1 in which the CIE coordinates alter from (0.33, 0.62) to (0.37, 0.60). The table also confirms that the $x$$Er^{3+}$/3$Yb^{3+}$ co-doped phosphors show efficient color tunability with the concentration of the Er^{3+} ion. It is also interesting to note from Fig. 13(b) that color tunability is not only observed due to variation in the concentration of Er^{3+} ion but also on changing the incident pump powers of the 980 nm excitation source in the case of 0.7Er^{3+}/3Yb^{3+} co-doped phosphor. As the pump power is increased, the color emitted by the phosphor was tuned from red to yellowish green color followed by yellow color. The color tunability was also observed by Gao *et al.* in the Er^{3+} doped compound as a function of different pump powers.[35] Accordingly, the CIE coordinates of the phosphor are shifted from (0.42, 0.41) to (0.40, 0.57). The calculated CIE coordinates for different pump powers are further given in

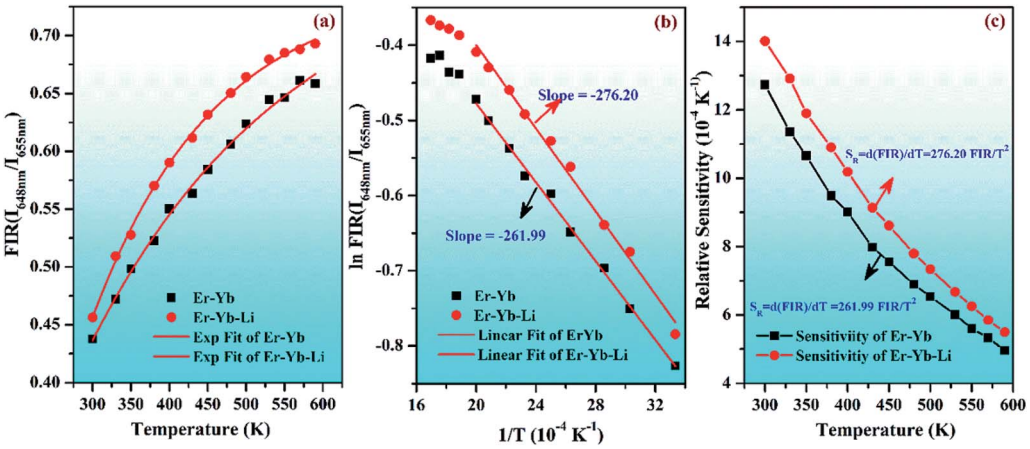

Fig. 17 (a) Plots of FIR (I_{648nm}/I_{655nm}) *versus* temperature, (b) ln FIR (I_{648nm}/I_{655nm}) *versus* T^{-1}, and (c) sensitivity *versus* temperature for the 0.7Er^{3+}/Yb^{3+} and 0.7Er^{3+}/Yb^{3+}/Li^+ co-doped $ZnGa_2O_4$ phosphors on excitation with 980 nm at 1 W.

Table 1. Thus, the fine color tunability has been achieved due to variation in the Er^{3+} ion concentrations and pump powers in the Er^{3+}/Yb^{3+} co-doped phosphor.

The correlated color temperature (CCT) has been calculated by using McCAMY's formula *via* taking the values of CIE coordinates. The CCT relation is given as:[72]

$$\mathrm{CCT} = 449n^3 + 3525n^2 + 6823.3n + 5520.33 \quad \text{(ii)}$$

where $n = (x - 0.3320)/(0.1858 - y)$ and (x, y) are the calculated CIE coordinates of the chosen phosphor samples. The values of the correlated color temperature were found to be 5551, 4216, 6601, 6379, and 4923 for the 0.7Er^{3+}, 0.3Er^{3+}/3Yb^{3+}, 0.5Er^{3+}/3Yb^{3+}, 0.7Er^{3+}/3Yb^{3+}, and 1.5Er^{3+}/3Yb^{3+} phosphor samples. The CCT values thus obtained at 6601 and 6379 K exist in the limit of cold light for the (0.39, 0.58) and (0.38, 0.59) CIE coordinates, respectively.

3.3.6 Lifetime measurements. The lifetimes of $^4S_{3/2}$ and $^4F_{9/2}$ levels for the $^4S_{3/2} \rightarrow {}^4I_{15/2}$ (554 nm) and $^4F_{9/2} \rightarrow {}^4I_{15/2}$ (655 nm) transitions have been monitored by chopping the continuous pulse of a 980 nm laser. The decay curves thus obtained for these transitions in the 0.7Er^{3+}, 0.7Er^{3+}/Yb^{3+}, and 0.7Er^{3+}/Yb^{3+}/Li^+ doped and co-doped $ZnGa_2O_4$ phosphors are shown in Fig. 14. The decay curves in these cases match well with mono-exponential fitting *via* the following equation:[6]

$$I = I_0 \exp(-t|\tau) \quad \text{(iii)}$$

where, I_0 and I are the emission intensities at the times of zero and t seconds, respectively, while τ is the lifetime of the emitting level. The lifetime (τ) values are found to be 149, 155, and 157 μs for the $^4S_{3/2} \rightarrow {}^4I_{15/2}$ (554 nm) transition whereas 163, 170, and 178 μs for $^4F_{9/2} \rightarrow {}^4I_{15/2}$ (655 nm) transition in the 0.7Er^{3+}, 0.7Er^{3+}/Yb^{3+}, and 0.7Er^{3+}/Yb^{3+}/Li^+ doped and co-doped $ZnGa_2O_4$ phosphors, respectively. It is noted from the figure that the presence of Yb^{3+} and Li^+ ions in the 0.7Er^{3+} doped $ZnGa_2O_4$ phosphor increases the lifetime of green and red emitting levels. However, the value of lifetime is relatively larger for Li^+ doping, which is due to increase in the crystallinity of the phosphor.[28,45] Thus, the increase in the values of lifetime is one of the factors responsible for improving the UC emission intensity of the 0.7Er^{3+} doped phosphor.

3.3.7 Optical heating in 0.7Er^{3+}/Yb^{3+} and 0.7Er^{3+}/Yb^{3+}/Li^+ co-doped phosphors. Optical heating arises due to non-radiative losses in transitions. It is a relative change in the UC emission intensities of TCLs of the Er^{3+}/Yb^{3+} co-doped phosphor. This induces UC-based FIR, which is a measure of optical heating in the sample. Many researchers have used TCLs of green emission to calculate FIR in the Er^{3+}/Yb^{3+} co-doped phosphor.[13,15,19,28] They have reported a variation in FIR with different pump powers. In our case, we have monitored the UC emission intensities of TCLs (*i.e.*, $^4F_{9/2}$(I) and $^4F_{9/2}$(II) levels) of red emission on excitation with 980 nm for 648 and 655 nm wavelengths, respectively. The UC emission intensity of the phosphor increases regularly with the increase in pump powers

Table 2 Comparison of relative sensitivity obtained in our case and reported by others

Rare earths	Host	Temperature	Relative sensitivity (S_R) (K^{-1}) at temp. (K)	Ref.
Er^{3+}, Yb^{3+}	$BaMoO_4$	200–300	0.0015 (463)	27
Er^{3+}, Yb^{3+}	$Ba_5Gd_8Zn_4O_{21}$	200–490	0.0031 (200)	34
Er^{3+}, Yb^{3+}, Eu^{3+}	Y_2O_3	301–403	0.0008 (427)	74
Er^{3+}, Yb^{3+}, Nd^{3+}	Y_2SiO_5	298–753	0.00095 (403)	75
Er^{3+}, Yb^{3+}	$ZnGa_2O_4$	300–600	0.00127 (300)	Present work
Er^{3+}, Yb^{3+}, Li^+	$ZnGa_2O_4$	300–600	0.00140 (300)	Present work

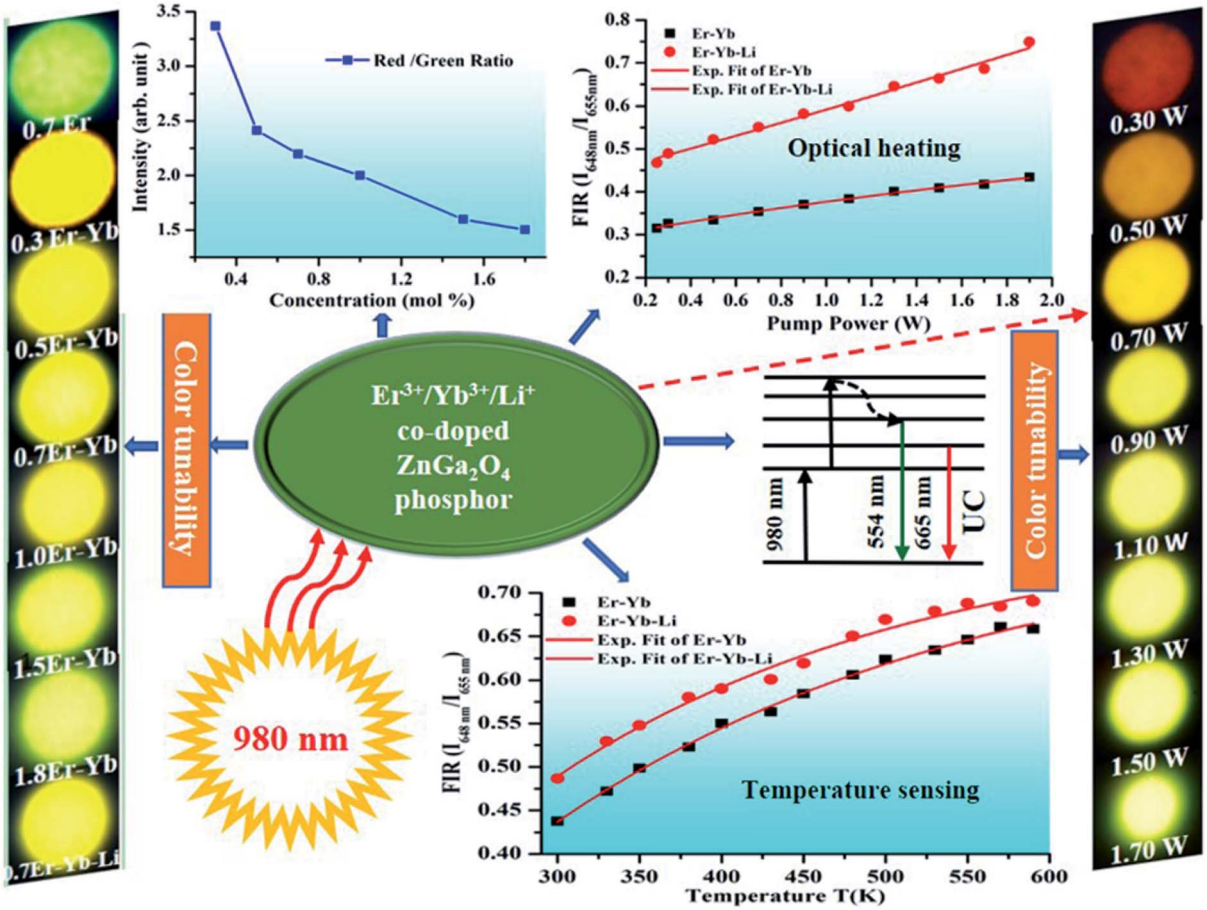

Fig. 18 Schematic model for color tunability, R/G ratio, energy level diagram, optical heating, and temperature sensing of the $Er^{3+}/Yb^{3+}/Li^{+}$ co-doped $ZnGa_2O_4$ phosphor.

(see Fig. 11). Zhang *et al.* have also observed an increase in the UC intensity of the red emission with the incident pump power.[25] It has been observed that the relative UC emission intensities of TCLs of red emission varies with the incident pump power. Fig. 15 shows the plots between FIR (I_{648nm}/I_{655nm}) and pump power for the $0.7Er^{3+}/Yb^{3+}$ and $0.7Er^{3+}/Yb^{3+}/Li^{+}$ co-doped $ZnGa_2O_4$ phosphors upon 980 nm excitation. When the pump power of the laser source is increased, the FIR also increases simultaneously.[28] The experimental profiles of FIR are exponentially well fitted in both the cases. The $0.7Er^{3+}/3Yb^{3+}/5Li^{+}$ co-doped phosphor gives a larger value of FIR because this phosphor emits a larger UC emission intensity compared to that of the $0.7Er^{3+}/Yb^{3+}$ co-doped phosphor. This is due to increase in the crystallinity and lifetime of the red emitting level.

Actually, the red emission of the Er^{3+} ion has Stark components at 648 and 655 nm wavelengths. They are well separated by an energy gap of 165 cm^{-1} and can be used as TCLs (*i.e.*, $^4F_{9/2}$(I) and $^4F_{9/2}$(II) levels). At lower pump power, the UC emission intensity of the 655 nm emission band is larger than that of the 648 nm emission band. Initially, the population of the excited ions is larger in the $^4F_{9/2}$(II) level compared to the $^4F_{9/2}$(I) level. This is responsible for larger UC intensity of the 655 nm emission band. When the incident pump power is further increased, the population of some of the ions is shifted towards the $^4F_{9/2}$(I) level. This induces a variation in the UC emission intensities for the 648 and 655 nm wavelengths in both the cases. This gives rise to FIR (I_{648nm}/I_{655nm}), which increases exponentially with the increase in pump power. The $0.7Er^{3+}/Yb^{3+}/Li^{+}$ co-doped phosphor shows increasing FIR values even at higher pump powers. Thus, these phosphors may be used for fabricating optical heating devices.

3.3.8 Effect of temperature on the UC intensity of the red region. We also studied the effect of external temperature on the intensity of red emission. The UC emission intensities of the TCLs of red emission was monitored at different external temperatures in the two cases, *viz.*, $0.7Er^{3+}/Yb^{3+}$ and $0.7Er^{3+}/Yb^{3+}/Li^{+}$ co-doped $ZnGa_2O_4$ phosphors. The UC emission intensity of the phosphor varies continuously with the rise in temperature. Fig. 16 shows the variation in UC emission intensity of the $0.7Er^{3+}/Yb^{3+}$ and $0.7Er^{3+}/Yb^{3+}/Li^{+}$ co-doped $ZnGa_2O_4$ phosphors monitored in the range of 625–700 nm on increasing the external temperature upon 980 nm excitation at 1 W pump power. When the temperature of the phosphor sample increases, the UC emission intensity is found to decrease exponentially. It is due to increase of lattice vibrations in the phosphor samples. However, the emission intensity of

the 0.7Er^{3+}/Yb^{3+} co-doped phosphor is larger in the case of Li^+ doping and it is smaller for the pure phosphor. This is due to the fact that the lattice vibration of the phosphor increases with the rise in temperature. The non-radiative relaxations of the ions become more effective at higher lattice vibrations in the excited energy levels. As a result, the UC emission intensity of the phosphors decreases regularly, which has been well established in Fig. 16.

3.3.9 Temperature sensing in the 0.7Er^{3+}/Yb^{3+} and 0.7Er^{3+}/Yb^{3+}/Li^+ co-doped phosphors. Temperature sensing is generally based on FIR values obtained from the UC emission intensities of TCLs, as has been discussed earlier. The UC emission intensities of the TCLs vary with the rise in external temperature of the phosphor samples. The phosphor samples are heated externally and the corresponding temperature is measured using thermo-state arrangement. The temperature sensing sensitivity has been extensively investigated by various researchers in the Er^{3+}/Yb^{3+} co-doped phosphors.[3,23–28] They monitored the UC emission intensities of TCLs of green emission and used it for temperature sensing. They also reported a decrease in the UC emission intensity on increasing the temperature. In our case, we have monitored the UC emission intensities of TCLs of red emission band with the increase in temperature (*i.e.*, 300–600 K) of 0.7Er^{3+}/Yb^{3+} and 0.7Er^{3+}/Yb^{3+}/Li^+ co-doped $ZnGa_2O_4$ phosphors upon 980 nm excitation at 1 W. It has been observed that the UC emission intensities of the two TCLs of red emission band of Er^{3+} ion (*i.e.*, $^4F_{9/2}$(I) → $^4I_{15/2}$ (648 nm), $^4F_{9/2}$(II) → $^4I_{15/2}$ (655 nm)) decreases non-linearly as the temperature of the phosphors was increased. The UC intensities of the two TCLs were used to calculate the FIR in both the cases. The FIR (I_{648nm}/I_{655nm}) of the phosphors is found to increase exponentially with the rise in temperature and it is shown in Fig. 17(a). Actually, the rise in temperature of the phosphor leads to a shift in the population of ions in the two levels.[3] At low temperature, the lower TCL is largely populated and yields larger UC emission intensity for the 655 nm emission band. However, these populations are slightly shifted to higher TCL due to increase in the lattice vibrations at higher temperatures, as the lattice vibrations are strongly temperature dependent. This factor improves the UC emission intensity of the 648 nm emission band. Though, the UC emission intensity of the 655 nm emission band is larger than the 648 nm emission band. The overall UC emission intensity of these TCLs decreases due to non-radiative relaxation of the ions, whereas the FIR (I_{648nm}/I_{655nm}) of the phosphors increases dramatically. Accordingly, the FIR originating from the two TCLs of the Er^{3+} ions, *i.e.*, $^4F_{9/2}$(I) and $^4F_{9/2}$(II), obeys the Boltzmann distribution law and can be mathematically expressed as:

$$\mathrm{FIR} = \frac{I_2}{I_1} = \frac{N_2}{N_1} = A\ \exp\left(-\frac{\Delta E}{kT}\right) + B \qquad \text{(iv)}$$

where I_1 (lower level) and I_2 (upper level) represent the integrated UC emission intensities of the two TCLs, while N_1 and N_2 are the corresponding number of ions, respectively. A and B are the fitting constants and overlap of the luminescence peaks, respectively. The constant (k) is Boltzmann's constant with its value of 0.695 cm^{-1} K^{-1}, T is absolute temperature, and ΔE is the energy difference between the two TCLs of $^4F_{9/2}$(I) and $^4F_{9/2}$(II) of the Er^{3+} ions, respectively. The FIR plots are found to fit exponentially with temperature in the two cases using relation (iv).

Fig. 17(b) shows a plot between log(FIR) and T^{-1} of red UC emission intensity in the range of 300–600 K for the 0.7Er^{3+}/3Yb^{3+} and 0.7Er^{3+}/3Yb^{3+}/5Li^+ co-doped $ZnGa_2O_4$ phosphors. The experimental data are found to vary non-linearly. The plot between logarithmic of FIR *versus* inverse of absolute temperature (T^{-1}) was assumed to calculate the slope values and they were found to be 261.99 and 276.20 for the 0.7Er^{3+}/3Yb^{3+} and 0.7Er^{3+}/3Yb^{3+}/5Li^+ co-doped phosphors, respectively. The energy band gap (ΔE) has been evaluated by multiplying the slope values with $k = 0.695$ cm^{-1} K^{-1} and their values are found to be 182.08 and 191.96 cm^{-1} for the 0.7Er^{3+}/3Yb^{3+} and 0.7Er^{3+}/3Yb^{3+}/5Li^+ co-doped phosphors, respectively.

The values of the relative sensitivity (S_R) and absolute sensitivity (S_A) can be calculated with the help of following relations:

$$S_R = \frac{\mathrm{d(FIR)}}{\mathrm{d}(T)} = \mathrm{FIR}\left(\frac{\Delta E_f}{kT^2}\right) \qquad \text{(v)}$$

$$S_A = \frac{1}{\mathrm{FIR}}\frac{\mathrm{d(FIR)}}{\mathrm{d}(T)} = \left(\frac{\Delta E_f}{kT^2}\right) \qquad \text{(vi)}$$

In these relations, all the terms have their usual meanings. The terms, S_R and S_A are dependent on ΔE_f. The calculated relative sensitivity (S_R) as a function of different temperatures is shown in Fig. 17(c). The rate of change of FIR as a function of temperature is termed as sensitivity. The relative sensitivity decreases continuously with increasing the temperature within the measured temperature range, *i.e.*, 300–600 K. The figure also shows that the relative sensitivity (S_R) is maximum at 300 K in both the cases and their values are found to be 0.00127 and 0.00140 K^{-1} for the 0.7Er^{3+}/Yb^{3+} and 0.7Er^{3+}/Yb^{3+}/Li^+ co-doped $ZnGa_2O_4$ phosphors, respectively. Wang *et al.* have also obtained larger value of temperature sensing sensitivity in the Er^{3+}/Yb^{3+} co-doped phosphor *via* doping of Ho^{3+} and Tm^{3+} ions.[73] The absolute sensitivity (S_A) has also been calculated using relation (vi) for the 0.7Er^{3+}/Yb^{3+} and 0.7Er^{3+}/Yb^{3+}/Li^+ co-doped $ZnGa_2O_4$ phosphors and their values were obtained as 0.00291 and 0.00307 K^{-1}, respectively. Thus, the Li^+ ion improves the value of relative sensitivity (S_R) and absolute sensitivity (S_A) in the 0.7Er^{3+}/Yb^{3+} co-doped phosphor. The relative sensitivity obtained in our case has been compared with reported sensitivities by other values and they are summarized in Table 2. The table also reveals that the relative sensitivity observed in our case is very close to the value reported by others.

The term (ΔE_f) is the fitting energy difference between the two TCLs. The error (δ) with respect to the actual experimental energy difference (ΔE_m) gives an insight of its agreement with the fitting energy difference (ΔE_f). The error (δ) can be expressed by the following relation:[14]

$$\delta = \frac{|\Delta E_f - \Delta E_m|}{\Delta E_m} \qquad \text{(vii)}$$

where ΔE_m is the actual measured value from the two TCLs of Er^{3+} ion. The error (δ) is an important factor that can be determined if and only if the value of ΔE_f comes close to an agreement with the experimentally observed value of ΔE_m. If the value of δ is observed to be large, it shows that there is a possibility of energy transfer between TCLs and other levels.[14] It also reveals that the number of ions present in the TCLs is due to the combined effect of Boltzmann distribution and energy transfer at higher temperatures. The values of (δ) are found to be 10% and 16%, for the $0.7Er^{3+}/Yb^{3+}$ and $0.7Er^{3+}/Yb^{3+}/Li^{+}$ co-doped $ZnGa_2O_4$ phosphors, respectively, in the range of 300–600 K.

We have summarized the whole mechanisms by using a schematic model and it is shown in Fig. 18. The figure shows not only the color tunability with different concentrations and pump powers but also the red to green ratio for different concentrations of Er^{3+} ions, induced optical heating, and temperature sensing characteristics. This figure also shows the energy level diagram representing the upconversion (UC) emissions in green and red regions upon 980 nm excitation.

4. Conclusions

Upconversion luminescence has been studied in the $Er^{3+}/Yb^{3+}/Li^{+}$ co-doped $ZnGa_2O_4$ phosphor. The structural characterization shows a better crystallinity in the presence of Li^{+} ions. The absorption spectra show a large number of peaks due to Er^{3+} and Yb^{3+} ions. The Er^{3+}/Yb^{3+} co-doped phosphor gives an intense red UC emission on excitation with 980 nm. The luminescence intensity *versus* pump power dependent plot proves the requirement of two photons for this emission. The phosphor also shows color tunability due to change in Er^{3+} ion concentration and incident pump power. The presence of Li^{+} ions in the Er^{3+}/Yb^{3+} co-doped phosphor enhances the UC emission intensity more than two times. The lifetime of the levels of Er^{3+} ions is also increased in the presence of Li^{+} ions. The enhancement in the intensity is due to an increase in the crystallinity and particles size of the phosphor. The pump power induced FIR results in better optical heating in the phosphors. The Er^{3+}/Yb^{3+} and $Er^{3+}/Yb^{3+}/Li^{+}$ co-doped $ZnGa_2O_4$ phosphors show efficient temperature sensing sensitivity and the sensitivity is as high as 14×10^{-4} K^{-1} in the presence of Li^{+} ions. Thus, the $Er^{3+}/Yb^{3+}/Li^{+}$ co-doped $ZnGa_2O_4$ phosphor may be used in photonic, optical heating, and temperature sensing devices.

Conflicts of interest

The authors declare that there is no conflict of interest in the present study.

Acknowledgements

Ms Monika wishes to acknowledge Council of Scientific & Industrial Research (CSIR), India for financial assistance as Junior Research Fellow (Grant No. 09/013(0826)/2018-EMR-I). Dr A. Bahadur is thankful to DST-SERB, India for providing funds under the scheme "Empowerment and Equity Opportunities for Excellence in Science (File no. EEQ/2017/000757).

References

1 Q. Qiang and Y. Wang, *New J. Chem.*, 2019, **43**, 5011–5019.
2 R. S. Yadav, S. J. Dhoble and S. B. Rai, *Sens. Actuators, B*, 2018, **273**, 1425–1434.
3 X. Wang, Y. Wang, Y. Bu, X. Yan, J. Wang, P. Cai and H. J. Seo, *Sci. Rep.*, 2017, **7**, 43383.
4 N. Rakov and G. S. Maciel, *Sens. Actuators, B*, 2012, **164**, 96–100.
5 R. S. Yadav and S. B. Rai, *J. Alloys Compd.*, 2017, **700**, 228–237.
6 R. S. Yadav, R. V. Yadav, A. Bahadur and S. B. Rai, *RSC Adv.*, 2016, **6**, 51768–51776.
7 R. S. Yadav, S. J. Dhoble and S. B. Rai, *New J. Chem.*, 2018, **42**, 7272–7282.
8 S. P. Tiwari, S. K. Maurya, R. S. Yadav, A. Kumar, V. Kumar, M. F. Joubert and H. C. Swart, *J. Vac. Sci. Technol., B: Nanotechnol. Microelectron.: Mater., Process., Meas., Phenom.*, 2018, **36**, 060801.
9 S. Ye, F. Xiao, Y. X. Pan, Y. Y. Ma and Q. Y. Zhang, *Mater. Sci. Eng., R*, 2010, **71**, 1–34.
10 H. Dong, L. D. Sun and C. H. Yan, *Chem. Soc. Rev.*, 2015, **44**, 1608–1634.
11 J. Xue, X. Wang, J. H. Jeong and X. Ya, *Phys. Chem. Chem. Phys.*, 2018, **20**, 11516–11541.
12 M. Mondal, V. K. Rai and C. Srivastava, *Chem. Eng. J.*, 2017, **327**, 838–848.
13 P. Du, L. H. Luo, H. K. Park and J. S. Yu, *Chem. Eng. J.*, 2016, **306**, 840–848.
14 X. Wang, Q. Liu, Y. Bu, C. S. Liu, T. Liu and X. Yan, *RSC Adv.*, 2015, **5**, 86219–86236.
15 S. Dong, J. Xu, T. Jia, M. Xu, C. Zhong, G. Yang, J. Li, D. Yang, F. He, S. Gai, P. Yang and J. Lin, *Chem. Sci.*, 2019, **10**, 4259–4271.
16 Y. Zhang, S. Xu, X. Li, J. Zhang, J. Sun, H. Xia, R. Hua and B. Chen, *Opt. Mater. Express*, 2018, **8**, 368–384.
17 R. S. Yadav, R. K. Verma, A. Bahadur and S. B. Rai, *Spectrochim. Acta, Part A*, 2015, **142**, 324–330.
18 J. Zhou, Y. Sun, X. Du, L. Xiong, H. Hu and F. Li, *Biomaterials*, 2010, **31**, 3287–3295.
19 X. Ai, C. J. H. Ho, J. Aw, A. B. E. Attia, J. Mu, Yu. Wang, X. Wang, Y. Wang, X. Liu, H. Chen, M. Gao, X. Chen, E. K. L. Yeow, G. Liu, M. Olivo and B. Xing, *Nat. Commun.*, 2016, **7**, 10432.
20 R. S. Yadav, R. K. Verma and S. B. Rai, *J. Phys. D: Appl. Phys.*, 2013, **46**, 275101.
21 R. S. Yadav, R. K. Verma, A. Bahadur and S. B. Rai, *Spectrochim. Acta, Part A*, 2015, **137**, 357–362.
22 R. S. Yadav and S. B. Rai, *J. Lumin.*, 2017, **190**, 171–178.
23 H. Wang, X. Yin, M. Xing, Y. Fu, Y. Tian, X. Feng, T. Jiang and X. Luo, *J. Am. Ceram. Soc.*, 2018, **101**, 865–873.
24 K. Pavani, J. Suresh Kumar, K. Srikanth, M. J. Soares, E. Pereira, A. J. Neves and M. P. F. Graça, *Sci. Rep.*, 2017, **7**, 17646.

25 G. Zhang, Q. Qiang, S. Du and Y. Wang, *RSC Adv.*, 2018, **8**, 9512–9518.
26 Z. Wang, H. Jiao and Z. Fu, *Inorg. Chem.*, 2018, **57**, 8841–8849.
27 N. H. Belkhir, A. Toncelli, A. K. Parchur, E. Alvesc and R. Maalej, *Sens. Actuators, B*, 2017, **248**, 769–776.
28 R. S. Yadav, D. Kumar, A. K. Singh, E. Rai and S. B. Rai, *RSC Adv.*, 2018, **8**, 34699–34711.
29 D. R. Kim, S. W. Park, B. K. Moon, S. H. Park, J. H. Jeong, H. Choi and J. H. Kim, *RSC Adv.*, 2017, **7**, 1464–1470.
30 C. Mi, J. Wu, Y. Yang, B. Han and J. Wei, *Sci. Rep.*, 2016, **6**, 22545.
31 A. Maurya, R. S. Yadav, R. V. Yadav, A. Bahadur and S. B. Rai, *RSC Adv.*, 2016, **6**, 113469–113477.
32 J. Zhang, Z. Hao, J. Li, X. Zhang, Y. Luo and G. Pan, *Light: Sci. Appl.*, 2015, **4**, e239.
33 Q. Xiao, Y. Zhang, H. Zhang, G. Dong, J. Han and J. Qiu, *Sci. Rep.*, 2016, **6**, 31327.
34 H. Suo, C. Guo and T. Li, *J. Phys. Chem. C*, 2016, **120**, 2914–2924.
35 D. Gao, X. Zhang, Q. Pang, J. Zhao, G. Xiao and D. Tian, *J. Mater. Chem. C*, 2018, **6**, 8011–8019.
36 Y. Cheng, K. Sun and P. Ge, *Optik*, 2018, **170**, 1–9.
37 J. H. Chung, J. H. Ryu, J. W. Eun, J. H. Lee, S. Y. Lee, T. H. Heo and K. B. Shim, *Mater. Chem. Phys.*, 2012, **134**, 695–699.
38 X. Gao, X. Liu, Q. Wen, X. Yang and S. Xiao, *J. Appl. Phys.*, 2014, **116**, 173105.
39 L. Jiang, S. Xiao, X. Yang, J. Ding and K. Dong, *Appl. Phys. B*, 2012, **107**, 477–481.
40 V. Singh, V. K. Rai, I.-J. Lee, I. Ledoux-Rak, K. Al-Shamery, J. Nordmann and M. Haase, *Appl. Phys. B*, 2012, **106**, 223–228.
41 I. Kamińska, *et al.*, *RSC Adv.*, 2015, **5**, 78361–78373.
42 W. Yin, L. Zhao, L. Zhou, Z. Gu, X. Liu, G. Tian, S. Jin, L. Yan, W. Ren, G. Xing and Y. Zhao, *Chem.–Eur. J.*, 2012, **18**, 9239–9245.
43 D.-H. Kim, J. H. Ryu, J. H. Chung, K. B. Shim and S.-Y. Cho, *J. Electrochem. Soc.*, 2011, **158**, J345–J348.
44 Z. Chen, T. Chen, W. Gong, W. Xu, D. Wang and Q. Wang, *J. Am. Ceram. Soc.*, 2013, **96**, 1857–1862.
45 G. Chen, H. Liu, H. Liang, G. Somesfalean and Z. Zhang, *J. Phys. Chem. C*, 2008, **112**, 12030–12036.
46 Y. Ding, X. Zhang, H. Gao, S. Xu, C. Wei and Y. Zhao, *J. Alloys Compd.*, 2014, **599**, 60–64.
47 C. Zhao, X. Kong, X. Liu, L. Tu, F. Wu, Y. Zhang, K. Liu, Q. Zeng and H. Zhang, *Nanoscale*, 2013, **5**, 8084–8089.
48 Y. Cheng, K. Sun and P. Ge, *Opt. Mater.*, 2018, **83**, 13–18.
49 M. Puddu, G. Mikutis, W. J. Stark and R. N. Grass, *Small*, 2016, **12**, 452–456.
50 C. D. S. Brites, X. Xie, M. L. Debasu, X. Qin, R. Chen, W. Huang, J. Rocha, X. Liu and L. D. Carlos, *Nat. Nanotechnol.*, 2016, **11**, 851–856.
51 Y. Gao, F. Huang, H. Lin, J. Zhou, J. Xu and Y. Wang, *Adv. Funct. Mater.*, 2016, **26**, 3139–3145.
52 P. Cai, X. Wang and H. J. Seo, *Phys. Chem. Chem. Phys.*, 2018, **20**, 2028–2035.
53 C. R. Garcia, J. Oliva, L. A. Diaz-Torres, E. Montes, G. Hirata, J. Bernal-Alvarado and C. Gomez-Solis, *Ceram. Int.*, 2019, **45**, 4972–4979.
54 J.-H. Lee, H.-J. Park, K. Yoo, B.-W. Kim, J. C. Lee and S. Park, *J. Eur. Ceram. Soc.*, 2007, **27**, 965–968.
55 W. Yang, J. Li, B. Liu, X. Zhang, C. Zhang, P. Niu and X. Jiang, *Nanoscale*, 2018, **10**, 19039–19045.
56 L. Zou, X. Xiang, M. Wei, F. Li and D. G. Evans, *Inorg. Chem.*, 2008, **47**(4), 1361–1369.
57 K.-H. Hsu, M.-R. Yang and K.-S. Chen, *J. Mater. Sci.*, 1998, **9**, 283–288.
58 S.-H. Choe and M.-S. Jin, *J. Korean Phys. Soc.*, 2008, **53**, 3474–3478.
59 M. Vasile, P. Vlazan and N. M. Avram, *J. Alloys Compd.*, 2010, **500**, 185–189.
60 M. Vasile, P. Vlazan, P. Sfirloaga, I. Grozescu, N. M. Avram and E. Rusu, *Phys. Scr.*, 2009, **135**, 014046.
61 M. Vasile, P. Vlazan, I. Grozescu and N. Avram, *Optoelectron. Adv. Mater., Rapid Commun.*, 2009, **3**, 1371–1374.
62 Y. He, M. Zhao, Y. Song, G. Zhao and X. Ai, *J. Lumin.*, 2011, **131**, 1144–1148.
63 R. S. Yadav, R. V. Yadav, A. Bahadur, T. P. Yadav and S. B. Rai, *Mater. Res. Express*, 2016, **3**, 036201.
64 X. Wang, Y. Wang, J. Yu, Y. Bu and X. Yan, *Opt. Express*, 2018, **26**, 21950–21959.
65 R. S. Yadav, Monika, E. Rai, L. P. Purohit and S. B. Rai, *J. Lumin.*, 2020, **217**, 116810.
66 D. L. Wood and J. Tauc, *Phys. Rev. B: Solid State*, 1972, **5**, 3144–3151.
67 Y. Zhang, H. Li, L. Shao, Z. Htwe and P. Yuan, *Opt. Mater. Express*, 2017, **7**, 3003–3010.
68 W. Wei, Y. Zhang, R. Chen, J. Goggi, N. Ren, L. Huang, K. K. Bhakoo, H. Sun and T. T. Y. Tan, *Chem. Mater.*, 2014, **26**, 5183–5186.
69 D. Li, W. Qin, P. Zhang, L. Wang, M. Lan and P. Shi, *Opt. Mater. Express*, 2017, **7**, 329–340.
70 E. F. Huerta, S. Carmona-Tellez, S. Gallardo-Hernandez, J. G. Cabanas-Moreno and C. Falcony, *ECS J. Solid State Sci. Technol.*, 2016, **5**, R129–R135.
71 S. Liu, S. Liu, M. Zhou, X. Ye, D. Hou and W. You, *RSC Adv.*, 2017, **7**, 36935–36948.
72 M. Rai, G. Kaur, S. K. Singh and S. B. Rai, *Dalton Trans.*, 2015, **44**, 6184–6192.
73 X. Wang, Y. Wang, J. M. Hueso and X. Yan, *Sci. Rep.*, 2017, **7**, 758.
74 R. Dey, A. Pandey and V. K. Rai, *Sens. Actuators, B*, 2014, **190**, 512–515.
75 N. Rakov and G. S. Maciel, *Opt. Lett.*, 2014, **39**, 3767–3769.